Collectivity in even $^{116}_{54}$Xe and $^{118}_{54}$Xe isotopes

J. M. Sears, D. B. Fossan, G. R. Gluckman, J. F. Smith, and I. Thorslund

Department of Physics and Astronomy, State University of New York at Stony Brook, Stony Brook, New York 11794

E. S. Paul

Oliver Lodge Laboratory, University of Liverpool, P.O. Box 147, Liverpool L69 7ZE, United Kingdom

I. M. Hibbert* and R. Wadsworth

Department of Physics, University of York, Heslington, York Y01 5DD, United Kingdom

High-spin states in the even ^{116}Xe and ^{118}Xe isotopes have been studied with the ^{58}Ni(^{64}Zn) reaction at 265 MeV using the GAMMASPHERE array. Several new rotational bands have been identified in these nuclei, and previously observed bands have been extended. In ^{116}Xe, a strongly coupled ($\Delta I = 1$) rotational band attributed to the $\nu[h_{11/2}(g_{7/2},d_{5/2})^1]$ configuration and a decoupled ($\Delta I = 2$) rotational band identified with the $\pi[h_{11/2}g_{7/2}]$ configuration have been found. Experimental observations also suggest that another rotational band may be understood within the framework of smooth band termination. In ^{118}Xe, two well-developed sidebands have been observed to decay by multiple paths to the yrast band at spins near $14\hbar$ and $28\hbar$. Identification of the higher-lying sideband has resulted in a substantial revision to the previously proposed spin extent of the yrast band, thereby resolving an earlier disgreement with theoretical calculations. [S0556-2813(98)06806-X]

PACS number(s): 21.10.Re, 25.70.Gh, 23.20.Lv, 27.60.+j

I. INTRODUCTION

Experimental investigations of nuclei located near the $Z = 50$ closed proton shell in the $A \approx 110$ mass region have uncovered exotic collective structures which coexist with the expected single-particle states. For example, well-deformed rotational bands built upon particle-hole (p-h) proton excitations across the shell gap have been observed recently in a number of $Z = 50-53$ nuclei [1–11] up to exceptionally high rotational frequencies. As additional particle alignment takes place at higher frequencies, many of these so-called "intruder bands" have displayed the characteristic effect of gradually decreasing dynamic moments of inertia to unusually low values. This feature has been attributed by theoretical calculations [12,13] to a mode of smooth band termination. In this interpretation, the nuclear shape traces a gradual (smooth) path through the triaxial γ plane from collective near-prolate ($\gamma \sim 0°$) to noncollective oblate ($\gamma = +60°$) as the available valence nucleons outside of the $Z = N = 50$ double shell-closure align. These rotational bands terminate once all of the spin vectors of the valence particles and holes in the underlying configurations have been aligned along the rotational axis. The observation of several rotational bands in the $Z = 52$ ^{114}Te$_{62}$ [7] and ^{116}Te$_{64}$ [8] isotopes which were interpreted within the framework of smooth band termination stimulated the present search for related structural features in the $Z = 54$ ^{116}Xe$_{62}$ and ^{118}Xe$_{64}$ isotopes. Indeed, the high-spin characteristics of the yrast band in the intermediate ^{117}Xe$_{63}$ isotope are suggestive of smooth band termination [14].

Well-deformed intruder rotational bands built upon $2p$-$2h$ proton excitations have been identified in many $_{50}$Sn, $_{51}$Sb, $_{52}$Te, and $_{53}$I nuclides in the $A \approx 110$ mass region. Among the even $^{106-118}$Sn [1,2,15–17] isotopes, collective rotational behavior has been found to be induced by the promotion of two protons from high-Ω, upsloping $g_{9/2}$ orbitals into low-Ω, downsloping $g_{7/2}$ orbitals, creating low-lying, deformed $2p2h$ $(\pi g_{7/2})^2 \otimes (\pi g_{9/2})^{-2}$ states. The slopes of these orbitals with respect to the quadrupole deformation parameter β_2 drive the nucleus towards a prolate deformation regulated by the $\pi g_{7/2}$-$\pi g_{9/2}$ level crossing at $\beta_2 \simeq 0.2$. In the odd $^{109-117}$Sb [4,5,18–20], even $^{110-116}$Te [6–8,21,22], and odd ^{113,115}I [10,11] isotopes, the $2p$-$2h$ proton excitation generates rotational bands built upon deformed $3p2h$, $4p2h$, and $5p2h$ proton configurations, respectively, with the additional valence proton(s) occupying deformation-driving $h_{11/2}$ or $g_{7/2},d_{5/2}$ orbitals. Given these observations, the $2p$-$2h$ proton excitation in the ^{116}Xe and ^{118}Xe isotopes would be expected to induce intruder rotational behavior based upon deformed $6p2h$ proton configurations, with the four additional valence protons occupying deformation-driving orbitals.

The present experiment was designed to investigate the mechanisms by which collective angular momenta are generated in the even ^{116}Xe and ^{118}Xe isotopes. In addition to intruder rotational bands, these isotopes are expected to manifest a wealth of interesting collective rotational structures generated by the four valence protons and available valence neutrons outside of the $Z = N = 50$ doubly-closed shell. As a result of this work, level schemes for both ^{116}Xe and ^{118}Xe have been established to high spins and excitation energies. In ^{116}Xe, a well-developed rotational band which may be understood within the framework of smooth band

———————
*Present address: Oliver Lodge Laboratory, University of Liverpool, P.O. Box 147, Liverpool L69 7ZE, United Kingdom.

TABLE I. Location θ of detector rings in the GAMMASPHERE array and the number of detectors N in each ring for this experiment. Angles θ are measured in degrees relative to the beam direction.

θ	N
17.3	2
31.7	5
37.4	5
50.1	5
58.3	1
79.2	1
90.0	6
99.3	1
100.8	1
121.7	5
129.9	10
142.6	5
148.3	4
162.7	5

termination has been identified. Decoupled ($\Delta I = 2$) and strongly coupled ($\Delta I = 1$) rotational bands also have been found. In ^{118}Xe, previously observed bands [23] have been extended, and several new bands have been identified. The yrast band also has been revised substantially [14] at spins greater than $26\hbar$, thereby resolving an earlier disagreement with theoretical calculations of the energy cost of high angular momenta [24].

A compilation of previous experimental information on ^{116}Xe and ^{118}Xe can be found in Refs. [25] and [26], respectively. Results of the two most recent high-spin γ-ray spectroscopy experiments utilizing the ^{90}Zr(^{31}P,pxn)^{116,118}Xe and ^{92}Mo(^{32}S,$2p\alpha$)^{118}Xe reactions are reported, respectively, in Refs. [14] and [23]. Preliminary results from the present independent study have been reported earlier [27,28].

II. EXPERIMENT

The ^{58}Ni(^{64}Zn) reaction at a beam energy of 265 MeV was used to populate states in the ^{116,118}Xe nuclei at the Lawrence Berkeley National Laboratory 88-In. Cyclotron facility. Two experiments were performed, one with a thin-target stack of two 500 μg/cm^2 self-supporting ^{58}Ni foils, and another using a 720 μg/cm^2 target of ^{58}Ni backed by a 19.2 mg/cm^2 layer of natural lead.

γ-ray transitions were detected with the GAMMASPHERE array which included 56 escape-suppressed HPGe detectors, each with an efficiency of approximately 75% of the standard 7.6 cm$\times$7.6 cm NaI(Tl) for a 1.33 MeV γ ray. The detectors were located in 14 rings which were distributed nearly uniformly over 4π solid angle, as indicated in Table I.

For the thin-target experiment, events in which at least four detectors fired in prompt coincidence were written to tape, and a total of 4.8×10^9 unfolded γ-γ-γ triple-coincidence events were collected. For the backed-target experiment, the fold condition was changed to require only three detectors firing in prompt coincidence, and a total of

0.45×10^9 unfolded γ-γ double-coincidence events were collected. In each experiment, approximately 20% (33%) of the events corresponded to the $\alpha 2p$ ($4p$) channel to ^{116}Xe (^{118}Xe). Considerable strength also was observed in the $3p$ channel to ^{119}Cs ($\sim$27%).

Recorded events from both experiments were separately unfolded off line into doubles and triples and replayed into E_γ-E_γ coincidence matrices and E_γ-E_γ-E_γ coincidence cubes, respectively. In addition, events from the thin-target experiment were sorted into double-gated matrices to select ^{116}Xe and, separately, ^{118}Xe preferentially from the populated reaction channels. Analysis was conducted using the programs ESCL8R and LEVIT8R [29].

Transition multipolarities for ^{116,118}Xe were determined from the backed-target data by using the method of directional correlation of oriented states (DCO) [30]. A matrix was constructed in which detectors situated at and near 90° with respect to the beam direction were sorted against those located at extreme forward ($\theta \leq 37.4°$) and extreme backward ($\theta \geq 142.6°$) angles. From this matrix, the angular-intensity ratio of γ rays

$$R_{\text{DCO}} = \frac{I_\gamma(\theta_{\text{fb}} - \overline{90°})}{I_\gamma(\overline{90°} - \theta_{\text{fb}})} \qquad (1)$$

was extracted, in which the second angle in parentheses refers to the matrix axis which is sliced by the gating transition, and $\overline{90°}$ and θ_{fb} represent those detectors located at and near 90° and at extreme forward and backward angles, respectively. In order to maximize the statistics available for angular-correlation analysis, two other matrices also were constructed, in which detectors located at extreme forward and backward angles, and detectors situated at and near 90°, were sorted against those located at all angles. From these matrices, the angular-intensity ratio

$$R'_{\text{DCO}} = \frac{I_\gamma(\theta_{\text{fb}} - \theta_{\text{all}})}{I_\gamma(\overline{90°} - \theta_{\text{all}})} \qquad (2)$$

was extracted, in which θ_{all} represents detectors at all angles. Angular-intensity ratios were calibrated using transitions of known multipolarity in the low excitation-energy region of the ^{118}Xe level scheme. Transitions of stretched quadrupole character were identified by the ratios R_{DCO} (R'_{DCO}) $\approx 1.0(4.0)$ when gated by a stretched $E2$. Similarly, the ratios R_{DCO} (R'_{DCO}) $\approx 0.5(2.0)$ indicated transitions of pure stretched dipole character. For γ-ray transitions in which both angular-intensity ratios could be extracted with adequate statistics, the ratios were found to imply consistent multipolarity assignments.

III. RESULTS

The level schemes for ^{116}Xe and ^{118}Xe based upon coincidence relationships and relative intensities as extracted from the present experiment are shown in Figs. 1 and 2, respectively. As seen in the figures, a total of 9 (11) sequences consisting of 4 or more levels were observed in ^{116}Xe (^{118}Xe); 6 new sequences have been identified in ^{116}Xe, and 4 new sequences have been found in ^{118}Xe. To
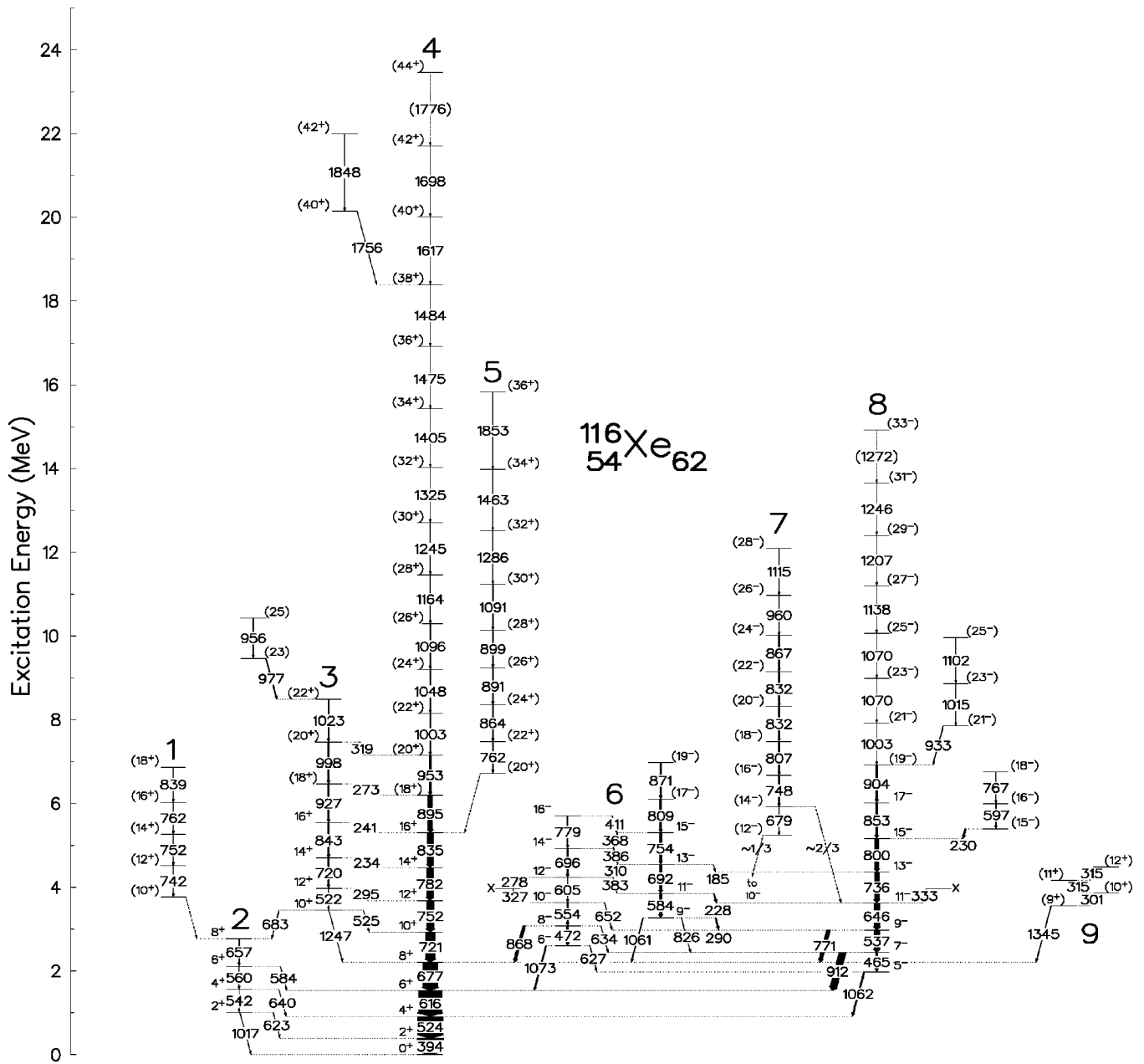
FIG. 1. Proposed level scheme for ^{116}Xe. Transition energies are given in keV. The width of each arrow is proportional to the intensity of the indicated transition. For clarity, the decay pattern of the level labeled with the letter X has been shown in two locations. Estimated spins of the unconnected bands are accurate to $\pm 2\hbar$.

facilitate this discussion, the observed level sequences have been numbered; hereinafter, these sequences will be referred to as ''bands'' regardless of the extent of collective behavior. Linking transitions to known lower-lying levels for bands 1, 5, and 7 in ^{116}Xe and band 5 in ^{118}Xe were not observed directly. Characteristics of the γ-ray transitions identified in these nuclei are listed in Tables II, III, IV, and V. In general, level spin and parity assignments were deduced from angular-correlation analysis and systematic decay properties. Spins for the unconnected bands have been estimated from the spins of the levels into which they decay, plus allowances for the angular momentum of the linking transitions; tentative parities have been assigned on the basis of decay considerations.

A. Level scheme for ^{116}Xe

The positive-parity yrast cascade in ^{116}Xe, labeled 4 in Fig. 1, has been extended [14] by six transitions to $I^{\pi} = (44^+)$. A spectrum generated for this band by the sum of two gates on the 1475- and 1484-keV band members in a double-gated matrix sorted to select ^{116}Xe preferentially is shown in Fig. 3. To construct this matrix, the original coincidence data from the thin-target experiment were sorted under a gating condition of two γ rays from a list of energies. This list included the energies of all members of the yrast band except for those of the 752-, 1475-, and 1484-keV transitions, which had contaminants at nearby energies, and also the 1776-keV transition, which was observed only tentatively. Although the spectrum shown in Fig. 3 cleanly illus-
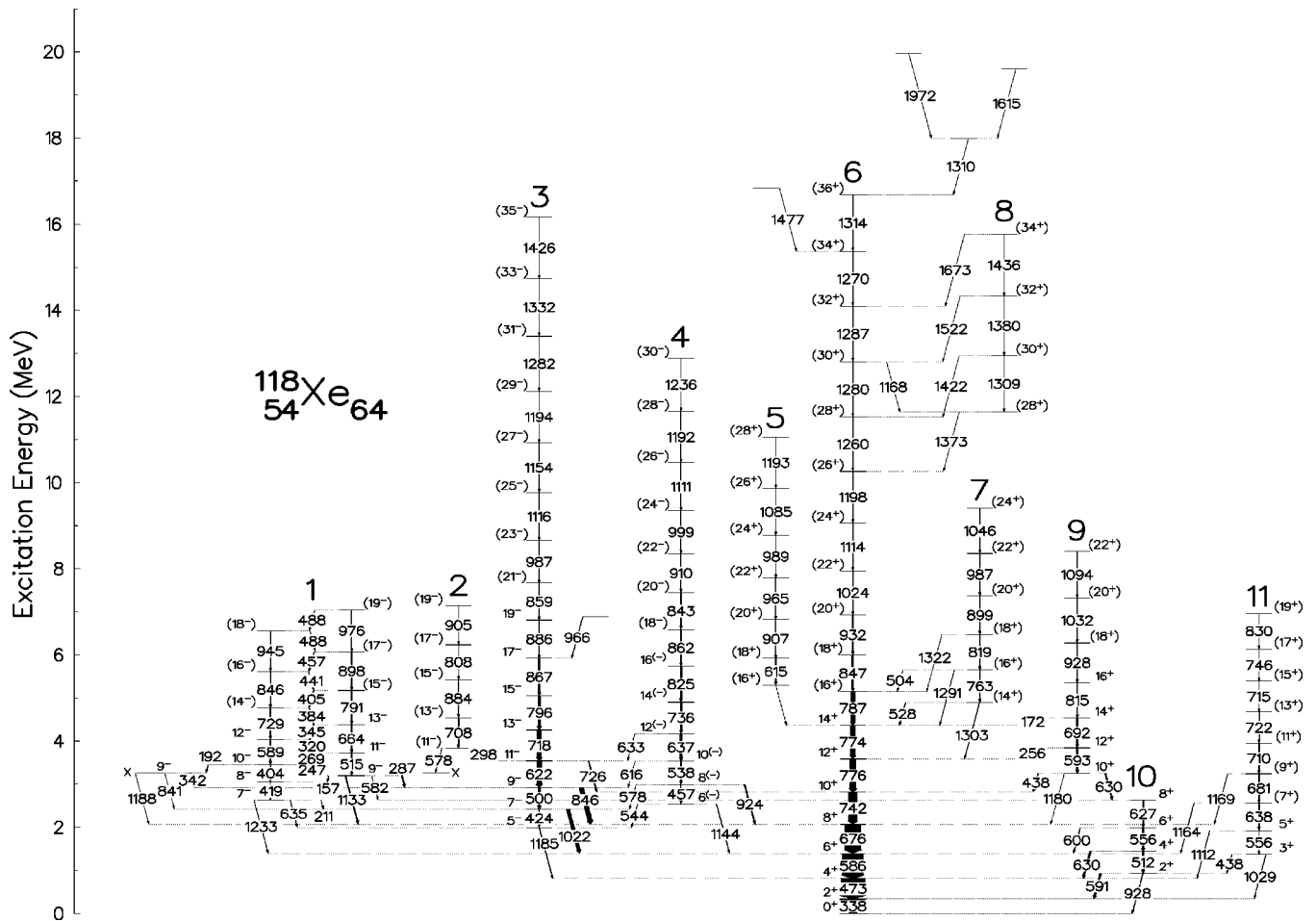
FIG. 2. Proposed level scheme for ^{118}Xe. Transition energies are given in keV. The width of each arrow is proportional to the intensity of the indicated transition. For clarity, the feeding pattern of the level labeled with the letter X has been shown in two locations. Estimated spins of the unconnected band are accurate to $\pm 2\hbar$.

trates the extent of the yrast band, the relative intensity of the 752-keV transition appears incorrect due to the absence of its energy from the sorting gate list. Also appearing in the spectrum displayed in Fig. 3 are two peaks at 1756 and 1848 keV. Further analysis using the double-gated matrix determined that these two transitions do not correspond to the favored continuation of the yrast band, but to a short sequence which decays to the (38^+) state of band 4, as has been indicated in Fig. 1. Reliable angular-correlation measurements could not be extracted for either these two transitions or any of the new transitions in band 4 owing to the weak intensities with which they were observed.

The band labeled 2 in Fig. 1 consists of three mutually coincident γ rays and decays via several weak transitions to band 4. Only the 657-keV transition in this band has not been observed before [25]. In the absence of reliable angular-correlation measurements, the spins and parity of this band have been assigned on the basis of the systematic behavior observed in heavier even Xe nuclei [23]. A band consisting of four weak transitions and labeled 1 in Fig. 1 appears to feed into band 2 at the $I^\pi = 8^+$ state; a definitive link could not be identified.

The band labeled 3 in Fig. 1, populated at approximately 5% of the intensity of band 4, includes seven levels and has been observed for the first time in this work. Except for the highest state, every state in band 3 decays both in band and

to the nearest level in band 4. The lowest state in band 3 has three separate decay paths: a 683-keV transition to the $I^\pi = 8^+$ state in band 2, a 1247-keV transition to the 8^+ state in band 4, and a 525-keV transition to the 10^+ state in band 4. Though each of these linking transitions is too weak to extract angular-correlation measurements, the competing decay paths limit the possible spin and parity assignments to the lowest state in the band. Angular-intensity ratios measured for the 295-keV link between band 3 and the 12^+ state in band 4 have the values $R_{\rm DCO} = 0.94 \pm 0.16$ and $R'_{\rm DCO} = 4.04 \pm 0.23$. In order to ensure experimentally reasonable multipolarities for the intraband 522-keV transition and the 1247-keV link between band 3 and band 4, the multipolarity of the 295-keV transition has been concluded to have dominant $I \rightarrow I$ $M1$ character, with small possible $E2$ admixtures; this results in a spin and parity assignment of $I^\pi = 10^+$ to the experimental bandhead. In general, angular-correlation analysis of intraband transitions was hindered by the presence of strong contaminants in band 4 at similar energies. Measurements extracted for the 234- and 241-keV links between band 3 and band 4 are consistent with $I \rightarrow I$ assignments within quoted errors. A short sequence consisting of two transitions at 977 and 956 keV has been observed to decay into the highest state in this band.

Another new feature of this level scheme, band 5 includes eight transitions and has been followed up to a rotational

TABLE II. γ-ray energies, intensities, and angular-correlation data for transitions assigned to ^{116}Xe.

E_γ (keV) [a]	I_γ (%) [b]	R_{DCO} [c]	R'_{DCO} [c]	$I_i^\pi \to I_f^\pi$	Multipolarity
184.8	1.1(0.1)		2.32(0.33)	$13^- \to 13^-$	$M1/E2$
227.8	3.7(0.1)		3.47(0.16)	$11^- \to 11^-$	$M1/E2$
230.1(0.7)	5.8(0.2)			$(15^-) \to 15^-$	$M1/E2$
233.7	2.3(0.1)	0.83(0.14)	3.00(0.19)	$14^+ \to 14^+$	$M1/E2$
241.4	1.7(0.1)		2.80(0.35)	$16^+ \to 16^+$	$M1/E2$
273.3(0.3)	0.8(0.1)			$18^+ \to 18^+$	$M1/E2.$
277.6	2.0(0.1)			$12^- \to$	
290.0	4.7(0.2)	0.96(0.12)	3.71(0.22)	$9^- \to 9^-$	$M1/E2$
295.4	2.2(0.1)	0.94(0.16)	4.04(0.23)	$12^+ \to 12^+$	$M1/E2$
301.2(1.4)	≤0.5			$(10^+ \to 9^+)$	$(M1/E2)$
309.5	4.6(0.5)	0.67(0.07)	2.44(0.14)	$13^- \to 12^-$	$M1/E2$
315.0(1.4) [d]	≤0.5 [d]			$(11^+ \to 10^+)$	$(M1/E2)$
315.0(1.4) [d]	≤0.5 [d]			$(12^+ \to 11^+)$	$(M1/E2)$
319.2(0.3)	1.4(0.1)			$20^+ \to 20^+$	$M1/E2$
327.4	≤0.5			$\to 10^-$	
332.6	2.2(0.1)			$\to 11^-$	
367.7	2.7(0.3)	0.66(0.07)	2.10(0.15)	$15^- \to 14^-$	$M1/E2$
382.6	1.1(0.1)	0.65(0.26)	2.56(0.45)	$12^- \to 11^-$	$M1/E2$
386.3	3.3(0.3)	0.72(0.07)	2.50(0.19)	$14^- \to 13^-$	$M1/E2$
393.6	104.6(1.9)	1.00 [e]	4.00 [e]	$2^+ \to 0^+$	$E2$
411.2	1.6(0.2)			$16^- \to 15^-$	$M1/E2$
465.2	6.4(0.2)	0.91(0.08)	3.82(0.18)	$7^- \to 5^-$	$E2$
472.0	7.3(0.6)		3.95(0.23)	$8^- \to 6^-$	$E2$
521.6	1.1(0.2)			$12^+ \to 10^+$	$E2$
524.2	100.0(3.2)	0.99(0.01)	3.99(0.03)	$4^+ \to 2^+$	$E2$
525.4(0.4)	≤0.5			$10^+ \to 10^+$	$M1/E2$
536.9	21.8(0.7)	0.97(0.06)	4.05(0.10)	$9^- \to 7^-$	$E2$
541.6	1.1(0.1)			$4^+ \to 2^+$	$E2$
554.3	5.3(0.3)	0.99(0.07)	3.78(0.12)	$10^- \to 8^-$	$E2$
560.4	2.9(0.2)			$6^+ \to 4^+$	$E2$
583.8	9.8(0.3)	1.01(0.08)	3.37(0.18)	$11^- \to 9^-$	$E2$
584.0	0.6(0.1)			$6^+ \to 6^+$	$M1/E2$
597.2(0.4)	2.9(0.1)			$(16^- \to 15^-)$	$M1/E2$
605.0	2.7(0.3)	0.96(0.16)	4.16(0.33)	$12^- \to 10^-$	$E2$
615.6	93.3(2.8)	0.99(0.01)	4.10(0.02)	$6^+ \to 4^+$	$E2$
622.8	≤0.5			$2^+ \to 2^+$	$M1/E2$
627.4	1.3(0.2)			$6^- \to 5^-$	$M1/E2$
634.0	1.5(0.2)			$8^- \to 7^-$	$M1/E2$
639.8	1.2(0.1)			$4^+ \to 4^+$	$M1/E2$
645.9	24.0(0.8)	0.91(0.02)	3.96(0.05)	$11^- \to 9^-$	$E2$
651.5	2.0(0.3)			$10^- \to 9^-$	$M1/E2$
656.5	2.7(0.1)			$8^+ \to 6^+$	$E2$
677.2	60.7(1.9)	0.95(0.02)	4.01(0.03)	$8^+ \to 6^+$	$E2$
682.5	1.3(0.1)			$10^+ \to 8^+$	$(M1/E2)$
692.2	9.5(1.0)	0.95(0.10)	3.65(0.24)	$13^- \to 11^-$	$E2$
696.0	5.8(0.6)	0.88(0.10)	3.48(0.20)	$14^- \to 12^-$	$E2$
720.0	4.7(0.2)			$14^+ \to 12^+$	$E2$
721.2	39.0(1.2)	0.96(0.02)	3.87(0.05)	$10^+ \to 8^+$	$E2$
735.7	20.0(0.6)			$13^- \to 11^-$	$E2$
751.7	31.2(1.0)	0.93(0.02)	3.80(0.09)	$12^+ \to 10^+$	$E2$
754.2	8.0(0.8)			$15^- \to 13^-$	$E2$
766.6(1.3)	1.1(0.3)			$(18^- \to 16^-)$	$(E2)$
771.1	14.2(0.6)	0.52(0.05)	2.18(0.08)	$9^- \to 8^+$	$E1$
779.1	4.3(0.4)			$16^- \to 14^-$	$E2$
782.1	25.8(0.8)		3.77(0.12)	$14^+ \to 12^+$	$E2$

Table II. (Continued).

E_γ (keV) [a]	I_γ (%) [b]	R_{DCO} [c]	R'_{DCO} [c]	$I_i^\pi \to I_f^\pi$	Multipolarity
799.6	15.8(0.5)	0.91(0.06)	3.64(0.11)	$15^- \to 13^-$	$E2$
808.7	7.2(0.2)		3.28(0.13)	$(17^-) \to 15^-$	$(E2)$
826.4	1.3(0.2)			$9^- \to 7^-$	$E2$
835.2	21.8(0.6)		3.59(0.19)	$16^+ \to 14^+$	$E2$
842.7	5.0(0.3)		4.13(0.56)	$16^+ \to 14^+$	$E2$
853.1	7.3(0.3)	1.00(0.13)	3.82(0.28)	$17^- \to 15^-$	$E2$
868.4	10.7(0.5)		3.29(0.19)	$8^- \to 8^+$	$E1$
871.4(0.3)	6.0(0.1)			$(19^- \to 17^-)$	$(E2)$
894.5	16.6(0.5)			$(18^+) \to 16^+$	$(E2)$
904.0	6.6(0.2)			$(19^-) \to 17^-$	$(E2)$
911.6	26.7(0.9)	0.54(0.02)	2.14(0.04)	$7^- \to 6^+$	$E1$
926.9	4.7(0.1)			$(18^+) \to 16^+$	$(E2)$
932.7(0.3)	2.2(0.2)			$(21^- \to 19^-)$	$(E2)$
952.6(0.3)	7.6(0.2)			$(20^+ \to 18^+)$	$(E2)$
955.6(1.2)	2.0(0.1)			$(25 \to 23)$	$(E2)$
977.0(1.2)	3.3(0.2)			$(23) \to 22^+$	(dipole)
998.3(0.4)	4.4(0.2)			$(20^+ \to 18^+)$	$(E2)$
1002.7(0.3)	3.5(0.1)			$(22^+ \to 20^+)$	$(E2)$
1003.0(1.2)	1.1(0.2)			$(21^- \to 19^-)$	$(E2)$
1015.3(0.3)	1.1(0.2)			$(23^- \to 21^-)$	$(E2)$
1016.6(1.4)	≤ 0.5			$2^+ \to 0^+$	$E2$
1023.1(0.3)	3.4(0.2)			$(22^+ \to 20^+)$	$(E2)$
1047.7(0.3)	2.9(0.1)			$(24^+ \to 22^+)$	$(E2)$
1061.3	3.0(0.1)			$9^- \to 8^+$	$E1$
1061.9	5.3(0.4)	0.56(0.04)	2.09(0.06)	$5^- \to 4^+$	$E1$
1070.0(1.4) [d]	1.3(0.2) [d]			$(23^- \to 21^-)$	$(E2)$
1070.0(1.4) [d]	1.3(0.2) [d]			$(25^- \to 23^-)$	$(E2)$
1073.4	4.7(0.3)		3.52(0.29)	$6^- \to 6^+$	$E1$
1095.8(0.7)	2.5(0.1)			$(26^+ \to 24^+)$	$(E2)$
1102.0(1.4)	≤ 0.5			$(25^- \to 23^-)$	$(E2)$
1138.0(1.2)	≤ 0.5			$(27^- \to 25^-)$	$(E2)$
1163.8(0.4)	2.1(0.2)			$(28^+ \to 26^+)$	$(E2)$
1207.0(1.2)	≤ 0.5			$(29^- \to 27^-)$	$(E2)$
1245.1(0.3)	1.4(0.2)			$(30^+ \to 28^+)$	$(E2)$
1246.0(1.2)	≤ 0.5			$(31^- \to 29^-)$	$(E2)$
1246.8	≤ 0.5			$10^+ \to 8^+$	$E2$
1272.0(1.2)	≤ 0.5			$(33^- \to 31^-)$	$(E2)$
1325.1(0.4)	1.2(0.1)			$(32^+ \to 30^+)$	$(E2)$
1344.5(1.4)	2.2(1.0)			$(9^+) \to 8^+$	$(M1/E2)$
1405.2(0.8)	1.1(0.2)			$(34^+ \to 32^+)$	$(E2)$
1475.3(1.4)	0.6(0.2)			$(36^+ \to 34^+)$	$(E2)$
1483.5(1.7)	≤ 0.5			$(38^+ \to 36^+)$	$(E2)$
1616.6(1.5)	≤ 0.5			$(40^+ \to 38^+)$	$(E2)$
1698.0(1.7)	≤ 0.5			$(42^+ \to 40^+)$	$(E2)$
1756(2)	≤ 0.5			$(40^+ \to 38^+)$	$(E2)$
1776(2)	≤ 0.5			$(44^+ \to 42^+)$	$(E2)$
1848(2)	≤ 0.5			$(42^+ \to 40^+)$	$(E2)$

[a]Energies are accurate to within ± 0.2 keV except where noted.

[b]Intensities are normalized to 100% for the 524.2-keV transition.

[c]Angular-correlation measurements have been extracted from backed-target experiment only. Measurements are not available for transitions that are either too weak and/or contaminated.

[d]Doublet; energy and intensity reported for composite peak because individual peaks could not be resolved unambiguously.

[e]Defined by systematics.

TABLE III. γ-ray energies, intensities, and angular-correlation data for transitions assigned to ^{118}Xe.

E_γ (keV) [a]	I_γ (%) [b]	R_{DCO} [c]	R'_{DCO} [c]	$I_i^\pi \to I_f^\pi$	Multiplicity
157.5	0.7(0.1)			$9^- \to 8^-$	$M1/E2$
172.0(1.0)	≤0.5			$14^+ \to 14^+$	$M1/E2$
192.0	1.8(0.1)		2.43(0.11)	$10^- \to 9^-$	$M1/E2$
211.2(0.6)	≤0.5			$7^- \to 7^-$	$M1/E2$
246.6	5.5(0.6)	0.83(0.03)	3.23(0.07)	$10^- \to 9^-$	$M1/E2$
255.8	1.5(0.3)	1.12(0.13)	3.86(0.22)	$12^+ \to 12^+$	$M1/E2$
268.9	4.5(0.5)	0.67(0.05)	2.80(0.09)	$11^- \to 10^-$	$M1/E2$
286.8	4.5(0.4)	0.93(0.09)	4.17(0.22)	$9^- \to 9^-$	$M1/E2$
297.5	1.3(0.2)			$(11^-) \to 11^-$	$(M1/E2)$
319.6	3.8(0.4)	0.77(0.05)	2.66(0.10)	$12^- \to 11^-$	$M1/E2$
337.5	100.0(4.0)	1.00 [d]	4.00 [d]	$2^+ \to 0^+$	$E2$
341.8	≤0.5			$(9^-) \to 9^-$	$(M1/E2)$
344.9	3.7(0.4)			$13^- \to 12^-$	$M1/E2$
384.5	1.6(0.2)			$(14^-) \to 13^-$	$(M1/E2)$
403.9	1.7(0.2)	0.85(0.06)	3.38(0.12)	$10^- \to 8^-$	$E2$
405.4(0.4)	1.7(0.2)			$(15^- \to 14^-)$	$(M1/E2)$
418.5	1.0(0.2)	0.72(0.12)	3.31(0.30)	$8^- \to 7^-$	$M1/E2$
423.6	1.8(0.2)		3.77(0.46)	$7^- \to 5^-$	$E2$
438.0	0.9(0.1)			$3^+ \to 2^+$	$M1/E2$
438.1	3.2(0.2)	1.00(0.12)	3.84(0.21)	$10^+ \to 10^+$	$M1/E2$
440.8(0.4)	1.0(0.1)			$(16^- \to 15^-)$	$(M1/E2)$
456.8(0.4)	0.7(0.1)			$(17^- \to 16^-)$	$(M1/E2)$
457.3	2.4 (0.3)		2.68(0.27)	$8^{(-)} \to 6^{(-)}$	$E2$
472.8	92.0(4.0)	0.97(0.01)	3.88(0.02)	$4^+ \to 2^+$	$E2$
488.1(0.4)	0.5(0.1)			$(18^- \to 17^-)$	$(M1/E2)$
488.1(0.4)	0.6(0.1)			$(19^- \to 18^-)$	$(M1/E2)$
500.4	10.0(0.3)	0.98(0.05)	4.07(0.09)	$9^- \to 7^-$	$E2$
504.1(0.4)	≤0.5			$(16^+ \to 16^+)$	$(M1/E2)$
512.4	5.8(0.6)	0.96(0.07)	3.10(0.13)	$4^+ \to 2^+$	$E2$
515.4	4.0(0.4)		3.85(0.25)	$11^- \to 9^-$	$E2$
528.2(0.4)	1.5 (0.2)			$(14^+) \to 14^+$	$(M1/E2)$
538.3	4.0(0.4)	1.08(0.14)	4.31(0.35)	$10^{(-)} \to 8^{(-)}$	$E2$
544.0(0.6)	0.8(0.1)			$6^{(-)} \to 5^-$	$(M1/E2)$
555.8	7.7(0.8)	1.05(0.06) [e]	3.69(0.11) [e]	$6^+ \to 4^+$	$E2$
555.9	1.1(0.2)	1.05(0.06) [e]	3.69(0.11) [e]	$5^+ \to 3^+$	$E2$
577.6	0.9(0.1)			$(11^-) \to 9^-$	$(E2)$
578.2(0.6)	≤0.5			$8^{(-)} \to 7^-$	$(M1/E2)$
582.4(0.6)	≤0.5			$9^- \to 8^+$	$E1$
586.4	80.0(3.4)	0.98(0.01)	4.01(0.03)	$6^+ \to 4^+$	$E2$
588.5	2.8(0.3)			$12^- \to 10^-$	$E2$
590.6	6.4(0.6)			$2^+ \to 2^+$	$M1/E2$
592.8	5.8(0.6)	1.03(0.10)	3.98(0.22)	$12^+ \to 10^+$	$E2$
599.8	2.4(0.3)			$6^+ \to 6^+$	$M1/E2$
616.3(0.6)	≤0.5			$10^{(-)} \to 9^-$	$(M1/E2)$
622.1	18.6(0.6)	0.96(0.03)	4.06(0.08)	$11^- \to 9^-$	$E2$
627.2	4.5(0.5)	1.10(0.12)	4.15(0.32)	$8^+ \to 6^+$	$E2$
629.8	4.4(0.4)	1.15(0.35)	4.64(0.93)	$10^+ \to 8^+$	$E2$
630.3	6.8(0.7)	0.98(0.16)	3.08(0.38)	$4^+ \to 4^+$	$M1/E2$
632.6(0.6)	≤0.5			$12^{(-)} \to 11^-$	$(M1/E2)$
634.8	1.1(0.2)			$7^- \to 5^-$	$E2$
637.3	8.0(0.6)	1.14(0.07)	4.24(0.16)	$12^{(-)} \to 10^{(-)}$	$E2$
637.9	4.1(0.3)			$(7^+) \to 5^+$	$(E2)$
664.2	4.2(0.4)		3.85(0.34)	$13^- \to 11^-$	$E2$
676.4	60.0(1.7)	0.97(0.02)	4.06(0.03)	$8^+ \to 6^+$	$E2$
680.9	2.8(0.3)			$(9^+ \to 7^+)$	$(E2)$

TABLE III. (Continued).

E_γ (keV) [a]	I_γ (%) [b]	R_{DCO} [c]	R'_{DCO} [c]	$I_i^\pi \to I_f^\pi$	Multipolarity
692.0	4.1(0.4)	1.07(0.10)	3.67(0.25)	$14^+ \to 12^+$	$E2$
708.0(0.4)	3.5(0.2)			$(13^- \to 11^-)$	$(E2)$
710.1	2.2(0.2)			$(11^+ \to 9^+)$	$(E2)$
715.1	0.8(0.2)			$(15^+ \to 13^+)$	$(E2)$
718.4	16.9(0.6)	0.98(0.07)	3.75(0.14)	$13^- \to 11^-$	$E2$
721.7	2.0(0.3)			$(13^+ \to 11^+)$	$(E2)$
726.2(0.4)	3.5(1.0)			$11^- \to 10^+$	$E1$
729.0	2.5(0.3)			$(14^- \to 12^-)$	$(E2)$
735.6(0.4)	6.8(0.7)		4.19(0.29)	$14^{(-)} \to 12^{(-)}$	$E2$
742.2	33.0(1.0)	0.94(0.03)	3.80(0.05)	$10^+ \to 8^+$	$E2$
746.0(1.0)	0.6(0.2)			$(17^+ \to 15^+)$	$(E2)$
762.5(0.4)	1.4(0.1)			$(16^+ \to 14^+)$	$(E2)$
774.4	18.0(0.6)	0.93(0.08)		$14^+ \to 12^+$	$E2$
775.9	24.0(0.8)	1.05(0.05)	4.03(0.15)	$12^+ \to 10^+$	$E2$
787.3	14.0(0.4)			$(16^+) \to 14^+$	$(E2)$
790.5(0.4)	2.6(0.3)			$(15^- \to 13^-)$	$(E2)$
795.9	9.8(0.3)	1.05(0.17)	3.73(0.13)	$15^- \to 13^-$	$E2$
807.6(0.4)	0.8(0.1)			$(17^- \to 15^-)$	$(E2)$
814.9(0.3)	3.0(0.4)		3.77(0.40)	$16^+ \to 14^+$	$E2$
818.6(0.4)	2.8(0.2)			$(18^+ \to 16^+)$	$(E2)$
825.2(0.4)	6.0(0.6)		3.24(0.52)	$16^{(-)} \to 14^{(-)}$	$E2$
830.0(1.0)	≤ 0.5			$(19^+ \to 17^+)$	$(E2)$
841.4(0.6)	≤ 0.5			$9^- \to 7^-$	$E2$
842.8(0.4)	2.6(0.2)			$(20^- \to 18^-)$	$(E2)$
845.9	16.6(0.6)	0.50(0.04)	1.96(0.07)	$9^- \to 8^+$	$E1$
846.4(0.4)	1.6(0.2)			$(16^- \to 14^-)$	$(E2)$
846.5(0.3)	6.9(0.3)			$(18^+ \to 16^+)$	$(E2)$
859.2(0.4)	1.6(0.2)			$(21^-) \to 19^-$	$(E2)$
862.0(0.4)	3.4(0.4)			$(18^-) \to 16^{(-)}$	$(E2)$
867.1	6.5(0.7)		3.88(0.34)	$17^- \to 15^-$	$E2$
883.6(0.4)	1.1(0.1)			$(15^- \to 13^-)$	$(E2)$
886.1	3.0(0.3)		3.25(0.31)	$19^- \to 17^-$	$E2$
897.7(0.4)	2.1(0.2)			$(17^- \to 15^-)$	$(E2)$
898.5(0.4)	2.3(0.2)			$(20^+ \to 18^+)$	$(E2)$
905.0(0.4)	0.6(0.1)			$(19^- \to 17^-)$	$(E2)$
909.8(0.4)	2.0(0.1)			$(22^- \to 20^-)$	$(E2)$
924.5	4.0(0.4)	0.97(0.12)	4.05(0.29)	$8^{(-)} \to 8^+$	$(E1)$
928.1	1.7(0.4)			$2^+ \to 0^+$	$E2$
928.3(0.4)	2.5(0.3)			$(18^+) \to 16^+$	$(E2)$
931.6(0.3)	4.8(0.2)			$(20^+ \to 18^+)$	$(E2)$
945.4(0.4)	1.3(0.1)			$(18^- \to 16^-)$	$(E2)$
966.4(0.4)	1.6(0.2)			$\to 17^-$	
975.8(0.4)	1.7(0.2)			$(19^- \to 17^-)$	$(E2)$
986.6(0.4)	1.3(0.1)			$(22^+ \to 20^+)$	$(E2)$
987.4(0.4)	0.8(0.1)			$(23^- \to 21^-)$	$(E2)$
999.0(0.4)	1.4(0.2)			$(24^- \to 22^-)$	$(E2)$
1021.8	12.2(0.5)	0.50(0.03)	2.02(0.05)	$7^- \to 6^+$	$E1$
1023.5(0.3)	3.0(0.3)			$(22^+ \to 20^+)$	$(E2)$
1028.8	1.3(0.2)			$3^+ \to 2^+$	$M1/E2$
1032.4(0.5)	1.8(0.4)			$(20^+ \to 18^+)$	$(E2)$
1046.0(0.4)	≤ 0.5			$(24^+ \to 22^+)$	$(E2)$
1094.0(1.0)	0.8(0.1)			$(22^+ \to 20^+)$	$(E2)$
1111.4(0.6)	1.5(0.3)			$(26^- \to 24^-)$	$(E2)$
1112.1	1.3(0.2)	0.89(0.19)	2.95(0.44)	$5^+ \to 4^+$	$M1/E2$

TABLE III. (Continued).

E_γ (keV) [a]	I_γ (%) [b]	R_{DCO} [c]	R'_{DCO} [c]	$I_i^\pi \to I_f^\pi$	Multipolarity
1113.5(0.4)	2.5(0.1)			$(24^+\to22^+)$	$(E2)$
1116.0(0.6)	0.6(0.1)			$(25^-\to23^-)$	$(E2)$
1132.9	3.5(0.3)	0.48(0.11)	2.00(0.15)	$9^-\to8^+$	$E1$
1143.6	1.7(0.2)		3.26(0.33)	$6^{(-)}\to6^+$	$(E1)$
1153.9(0.6)	$\leqslant 0.5$			$(27^-\to25^-)$	$(E2)$
1163.9	1.0(0.1)			$(7^+)\to6^+$	$(M1/E2)$
1167.6(0.7)	$\leqslant 0.5$			$(30^+\to28^+)$	$(E2)$
1168.5	0.8(0.1)			$(9^+)\to8^+$	$(M1/E2)$
1180.4(0.6)	$\leqslant 0.5$			$10^+\to8^+$	$E2$
1184.8	2.0(0.2)	0.46(0.18)	2.17(0.14)	$5^-\to4^+$	$E1$
1187.6(0.4)	$\leqslant 0.5$			$9^-\to8^+$	$E1$
1191.6(0.6)	1.0(0.2)			$(28^-\to26^-)$	$(E2)$
1194.0(0.6)	$\leqslant 0.5$			$(29^-\to27^-)$	$(E2)$
1197.9(0.4)	2.4(0.1)			$(26^+\to24^+)$	$(E2)$
1233.3	1.0(0.2)		2.67(0.48)	$7^-\to6^+$	$E1$
1236.0(0.8)	0.7(0.1)			$(30^-\to28^-)$	$(E2)$
1260.3(0.5)	1.3(0.1)			$(28^+\to26^+)$	$(E2)$
1269.6(0.5)	0.9(0.1)			$(34^+\to32^+)$	$(E2)$
1280.5(0.5)	1.2(0.1)			$(30^+\to28^+)$	$(E2)$
1281.6(0.6)	$\leqslant 0.5$			$(31^-\to29^-)$	$(E2)$
1286.6(0.5)	1.2(0.1)			$(32^+\to30^+)$	$(E2)$
1291.0(0.6)	0.8(0.1)			$(16^+)\to14^+$	$(E2)$
1303.2(0.6)	1.2(0.1)			$(14^+)\to12^+$	$(E2)$
1308.6(0.6)	$\leqslant 0.5$			$(30^+\to28^+)$	$(E2)$
1310.0(0.5)	$\leqslant 0.5$			$\to36^+$	
1313.9(0.5)	$\leqslant 0.5$			$(36^+\to34^+)$	$(E2)$
1322.4(0.6)	$\leqslant 0.5$			$(18^+\to16^+)$	$(E2)$
1331.6(1.0)	$\leqslant 0.5$			$(33^-\to31^-)$	$(E2)$
1373.0(0.5)	$\leqslant 0.5$			$(28^+\to26^+)$	$(E2)$
1380.1(0.5)	$\leqslant 0.5$			$(32^+\to30^+)$	$(E2)$
1421.6(0.5)	$\leqslant 0.5$			$(30^+\to28^+)$	$(E2)$
1426.3(1.0)	$\leqslant 0.5$			$(35^-\to33^-)$	$(E2)$
1436.0(0.5)	$\leqslant 0.5$			$(34^+\to32^+)$	$(E2)$
1476.7(0.5)	$\leqslant 0.5$			$\to34^+$	
1521.6(0.6)	$\leqslant 0.5$			$(32^+\to30^+)$	$(E2)$
1614.7(0.7)	$\leqslant 0.5$				
1672.9(0.6)	$\leqslant 0.5$			$(34^+\to32^+)$	$(E2)$
1971.9(0.7)	$\leqslant 0.5$				

[a]Energies are accurate to within ± 0.2 keV except where noted.

[b]Intensities are normalized to 100% for the 337.5-keV transition.

[c]Angular-correlation measurements have been extracted from backed-target experiment only. Measurements are not available for transitions that are either too weak and/or contaminated.

[d]Defined by systematics.

[e]Angular-correlation measurement reported for composite peak because individual peaks could not be resolved unambiguously.

frequency in excess of 0.90 MeV/$\hbar$. A spectrum generated in the thin-target cube from the sum of all combinations of double-coincidence gates among the members of this band is shown in Fig. 4. This spectrum illustrates that the energy separation of adjacent γ-ray transitions in the band increases with increasing transition energy. Band 5 appears to decay to the yrast $I^\pi = 16^+$ state, but could not be connected conclusively. Transitions which may be involved in the decay path are labeled with a question mark in Fig. 4. While the intensity observed in the band was not sufficient to extract reliable

angular-correlation measurements for any band member, the regular level spacings of the band, the relatively high energies of the intraband transitions, and the absence of any crossover transitions suggest that band 5 is a rotational cascade of stretched $\Delta I = 2$ electric quadrupoles. Kinematic $\mathcal{J}^{(1)} \approx (2I+1)\hbar^2/E_\gamma$ and dynamic $\mathcal{J}^{(2)} \approx 4\hbar^2/\Delta E_\gamma$ moments of inertia extracted for the band are plotted in Fig. 5.

Populated at approximately 22% intensity, the band labeled 8 in Fig. 1 has been extended [25] to $I^\pi = (33^-)$. Band

TABLE IV. γ-ray energies and intensities (in parentheses) for transitions assigned to unconnected bands in ^{116}Xe. Intensities are normalized to 100% for the 524.2-keV transition.

Band 1	Band 5	Band 7
742 (1.8)	762 (4.5)	679 (1.4)
752 (1.6)	864 (4.5)	748 (4.0)
762 (1.0)	891 (4.2)	807 (3.5)
839 (0.9)	899 (4.2)	832 (5.0) [a]
	1091 (3.0)	867 (2.5)
	1286 (1.7)	960 (1.0)
	1463 (0.7)	1115 (0.7)
	1853 ($\leqslant$0.5)	

[a]Doublet; energy and intensity reported for composite peak because individual peaks could not be resolved unambiguously.

8 decays to band 4 by strong transitions at 771 and 912 keV and also by a weaker transition at 1062 keV. The ratios R_{DCO} and R'_{DCO} extracted for these three linking transitions (see Table II) are consistent with stretched dipole assignments, indicating odd spins for the band. Negative parity has been assigned to this band on the basis of the systematic behavior observed in nearby even Xe isotopes [23]. Angular-correlation analysis supports stretched quadrupole assignments for transitions observed in the band at energies up to 853 keV. Two sequences, each consisting of three levels, decay to the 15^- and (19^-) states in band 8 by weak transitions at 230 and 933 keV, respectively. Tentative spins and parities for these two structures have been assigned on the basis of yrast arguments and decay considerations as reliable angular-correlation measurements could not be extracted for any of the linking transitions.

Band 6, which has been observed for the first time in this work, consists of two cascades of $\Delta I = 2$ transitions connected by a series of $\Delta I = 1$ transitions. As in band 3, the possible spin and parity assignments for the lowest state in the odd-spin sequence are limited by the several observed decay paths. Angular-intensity ratios measured for the 290-keV link to the 9^- state in band 8 have the values $R_{DCO} = 0.96 \pm 0.12$ and $R'_{DCO} = 3.71 \pm 0.22$. In order to ensure an experimentally reasonable multiplicity for the competitive

TABLE V. γ-ray energies and intensities (in parentheses) for transitions assigned to band 5 in ^{118}Xe. Intensities are normalized to 100% for the 337.5-keV transition.

615 (2.7)
907 (1.9)
965 (1.8)
989 (1.3)
1085 (0.8)
1193 ($\leqslant$0.5)

826-keV link to the 7^- state in band 8, the multipolarity of the 290-keV transition has been concluded to have dominant $I \rightarrow I$ $M1$ character, with small possible $E2$ admixtures; this results in a spin and parity assignment of 9^- to the lowest state in the odd-spin sequence. This sequence is connected to its even-spin analog by five low-energy transitions. Angular-intensity ratios could be extracted for all of these connecting transitions except the 411-keV crossover; these ratios are suggestive of $\Delta I = 1$ mixed $M1/E2$ multipolarity assignments. Spin and parity assignments for the even-spin sequence have been determined on this basis. In addition to the strong 290-keV link, band 6 decays to band 8 via several other relatively weaker links; the ratios R'_{DCO} extracted for the 228- and 185-keV links are consistent with $I \rightarrow I$ $M1$ multipolarity assignments (with small possible $E2$ admixtures) within statistical errors. Band 6 also decays by three separate transitions to band 4; the ratios R'_{DCO} measured for the the strongest of these at 868 and 1073 keV are consistent with $I \rightarrow I$ $E1$ multipolarity assignments. Angular-correlation analysis of the intraband transitions, where possible, supports stretched $E2$ assignments. Notably, the 12^- state in band 6 has several competitive decay paths through an intermediate level labeled X for clarity in Fig. 1; this level decays to the 10^- state in band 6 by a 327-keV transition.

Eight weakly observed transitions are included in band 7. Although the specific transitions involved in the decay of this new band could not be determined, two decay paths have been established. Approximately two-thirds of the band's intensity feeds out from the next-to-lowest state in the band to the $I^\pi = 11^-$ state in band 8, and the remaining one-third
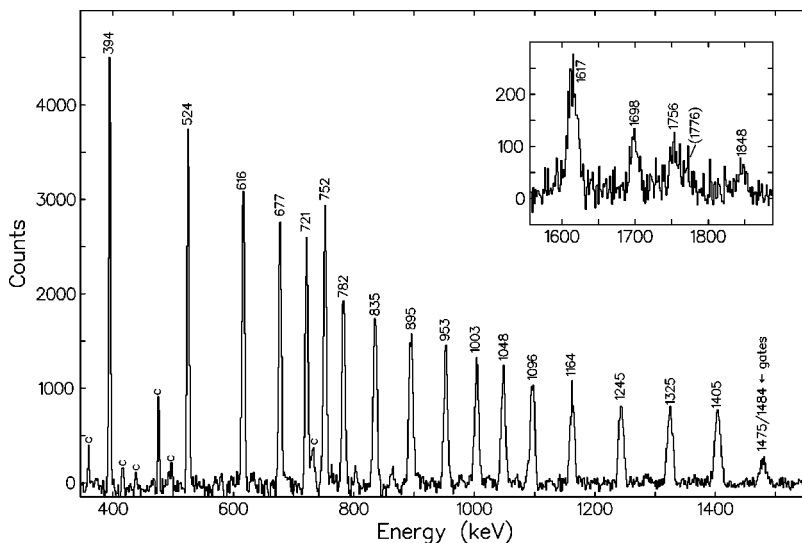
FIG. 3. Coincidence spectrum for band 4 in ^{116}Xe obtained from the sum of two gates on the 1475- and 1484-keV band members in a double-gated matrix sorted to select ^{116}Xe preferentially; see text for discussion. Band members are indicated by their energies, and contaminants are labeled with the letter C. Inset: spectrum at transition energies greater than 1550 keV.
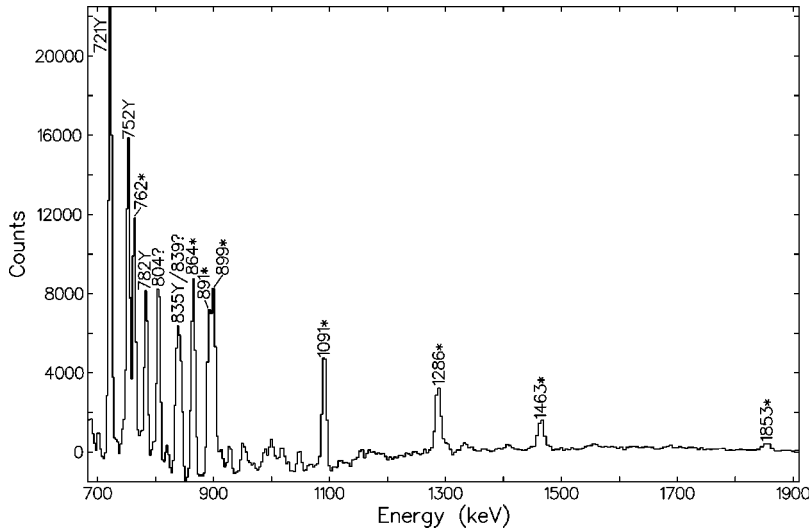
FIG. 4. Coincidence spectrum for band 5 in ^{116}Xe obtained from the sum of all intraband double gates in the thin-target cube. Band members are indicated by an asterisk, and transitions identified in band 4 (the yrast band) are indicated by the letter Y. Possible linking transitions between bands 4 and 5 are indicated with a question mark.

feeds out from the lowest state in the band to the 10^- state in band 6, as noted in Fig. 1. Experimental observations like those noted above in band 5 suggest that band 7 is also a rotational cascade of stretched $\Delta I=2$ electric quadrupoles.

Band 9 consists of three weak low-energy transitions which decay via a 1345-keV transition to the yrast 8^+ level. Tentative spin and parity assignments have been determined for this new band on the basis of yrast arguments and decay considerations.

In addition to the structures shown in Fig. 1, another sequence of mutually coincident γ rays was observed at approximately 5% of the intensity of band 4. This sequence, which could not be placed definitively in the level scheme, includes transitions at 737, 913, and 1150 keV.

B. Level scheme for ^{118}Xe

The positive-parity yrast cascade in ^{118}Xe, labeled 6 in Fig. 2, has been established to the $I^\pi=(36^+)$ level. A spectrum generated for this band by a gate on the 1198-keV band member in a double-gated matrix sorted to select ^{118}Xe preferentially is shown in Fig. 6. This matrix was constructed in a manner similar to that discussed above for the double-gated matrix in ^{116}Xe; in this case, the sorting gate list included the energies of all members of the yrast band up to spin (28^+), except for those of the 774- and 776-keV transitions, which had close-lying contaminants. The relative intensities of these two transitions appear incorrect in the spectrum displayed in Fig. 6 due to the absence of their energies from the sorting gate list. Spin and parity assignments in this band are supported up to the 14^+ state by angular-correlation analysis.

Evidence was presented in the most recent publication on ^{118}Xe [14] to support the continuation of the yrast cascade to $I^\pi=(46^+)$. Further analysis of this evidence in the present work using the double-gated matrix just described conclusively establishes that the γ-ray transitions proposed as this continuation actually form a parallel band which decays to various levels of band 6. Displayed in Fig. 2(b) of Ref. [14] is a spectrum of the yrast band generated by directly unfolding the original EUROGAM II data under a gating condition of any four of the strongest yrast transitions. Transitions observed in this spectrum at energies greater than 1350 keV were suggested as the continuation of the yrast band beyond

the (36^+) state. As seen here in the inset of Fig. 6, each of these transitions appears clearly in the 1198-keV gate in the double-gated matrix. While all of the labeled high-energy transitions have been attributed to ^{118}Xe, the extra gating condition available in the double-gated matrix permitted a conclusive determination of their placement in the level scheme. Four coincidence spectra gated on the 1373-, 1422-, 1522-, and 1673-keV transitions in the double-gated matrix are displayed in Figs. 7(a)–7(d), respectively. The appearance in these spectra of the 1260-, 1280-, and 1287-keV transitions in band 6 and the 1309-, 1380-, and 1436-keV transitions in band 8 documents the level ordering adopted in Fig. 2.

As noted above, band 8 decays by several high-energy transitions to band 6. Angular-correlation analysis of these
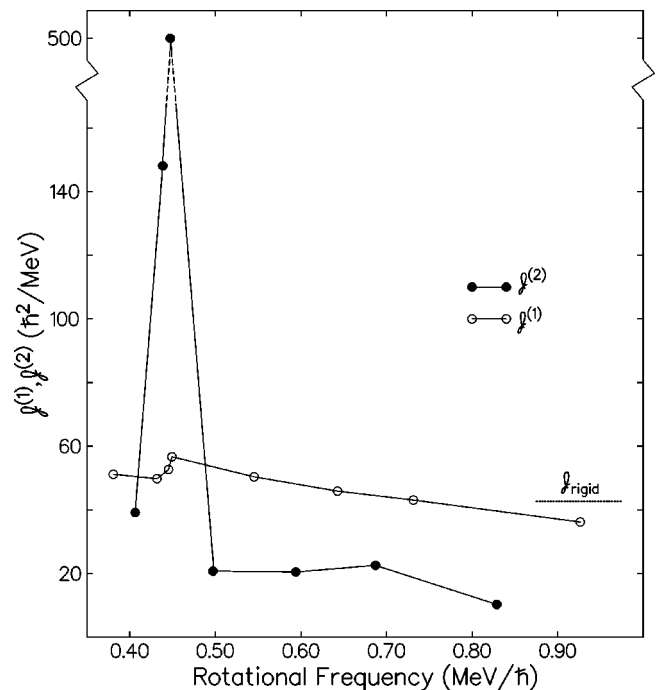
FIG. 5. Kinematic $\mathcal{J}^{(1)}$ and dynamic $\mathcal{J}^{(2)}$ moments of inertia extracted for band 5 in ^{116}Xe. A dashed line indicates the rigid-body moment of inertia calculated for a quadrupole deformation $\beta_2=0.2$.
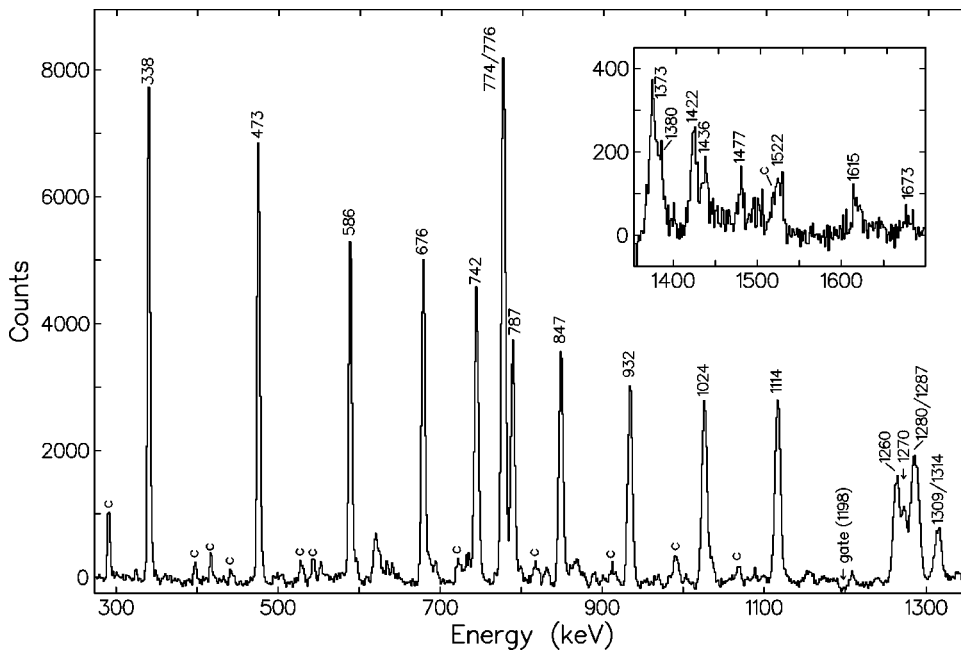
FIG. 6. Coincidence spectrum for band 6 in ^{118}Xe obtained from a gate on the 1198-keV band member in a double-gated matrix sorted to select ^{118}Xe preferentially; see text for discussion. Band members are indicated by their energies, and contaminants are labeled with the letter C. Inset: spectrum at transition energies greater than 1350 keV.

decay links was precluded by their weak observed intensities; however, identification of an 1168-keV transition connecting the $I^{\pi}=(30^{+})$ state in band 6 to band 8 does fix the relative spin and parity assignments of these two bands. Adjustment of either the relative spins or parities would require the observation of transitions described by experimentally unreasonable multipolarities.

The band labeled 7 in Fig. 2, populated at approximately 2.5% of the intensity of band 6, includes six levels and has been observed for the first time in this work. Two separate decay paths to the yrast cascade are observed for the lowest two states in this band: the experimental bandhead decays by 528- and 1303-keV transitions to the yrast $I^{\pi}=14^{+}$ and 12^{+} states, respectively, and the next higher state decays by 504- and 1291-keV transitions to the yrast (16^{+}) and 14^{+} states, respectively. Though each of these linking transitions was

too weak to extract reliable angular-correlation measurements, the observed decay pattern of this band limits the possible spin and parity assignments to the experimental bandhead. On the basis of systematics, this bandhead has been assigned to be (14^{+}); this represents the maximum spin allowed within the restriction imposed by the decay pattern. Intraband transitions also were too weak for angular-correlation analysis; they have been assumed to be stretched electric quadrupoles.

Band 5, also new, includes six transitions and appears to decay to the yrast $I^{\pi}=14^{+}$ state. The specific γ-ray transitions involved in the decay path of this band could not be identified conclusively. Although the intraband transitions were observed too weakly to measure angular-intensity ratios, experimental observations like those noted earlier in bands 5 and 7 in ^{116}Xe suggest that this band is also a rota-
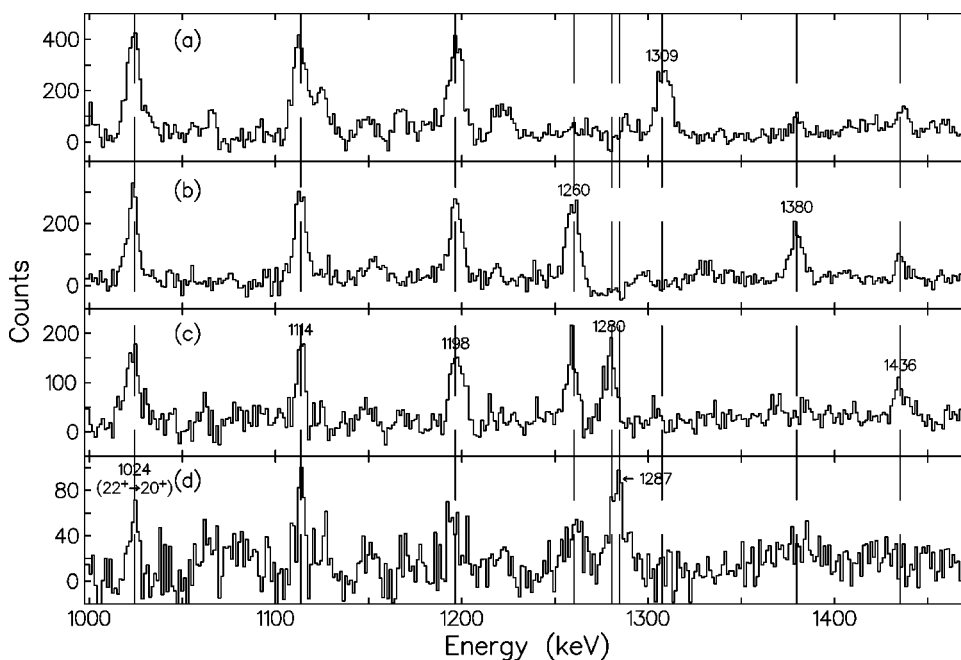
FIG. 7. Coincidence spectra generated in the ^{118}Xe double-gated matrix by gating on the 1373- (a), 1422- (b), 1522- (c), and 1673-keV (d) transitions linking band 8 to band 6. Note the staggered appearance of the yrast 1260-, 1280-, and 1287-keV transitions. Broken vertical lines have been drawn to guide the eye.
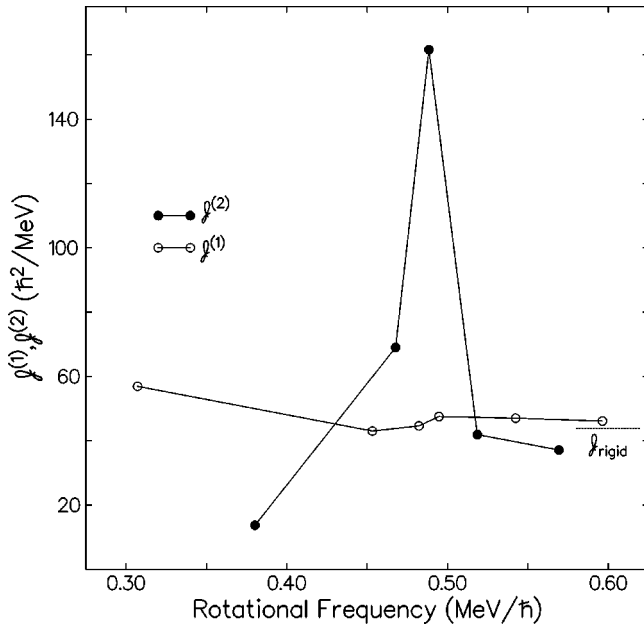
FIG. 8. Kinematic $\mathcal{J}^{(1)}$ and dynamic $\mathcal{J}^{(2)}$ moments of inertia extracted for band 5 in ^{118}Xe. A dashed line indicates the rigid-body moment of inertia calculated for a quadrupole deformation $\beta_2 = 0.2$.

tional cascade of stretched $\Delta I = 2$ electric quadrupoles. Kinematic $\mathcal{J}^{(1)}$ and dynamic $\mathcal{J}^{(2)}$ moments of inertia extracted for band 5 are plotted in Fig. 8.

Apart from band 2, all of the remaining features of ^{118}Xe shown in Fig. 2 have been investigated by Törmänen *et al.* in Ref. [23]. While many new transitions and decay paths have been found in the present work, our level scheme is consistent with that proposed earlier. As a result, we focus below on additions to the remaining features in the level scheme deduced from the present study.

Both of the negative-parity bands labeled 3 and 4 in Fig. 2 have been followed to higher spins. Populated at approximately 18% intensity, band 3 has been extended by three transitions to a level spin of $I^\pi = (35^-)$. Though considerably less intense than band 3, band 4 has been extended by four transitions to (30^-). Several new weak decay paths which connect band 4 to band 3 have been identified at 544, 578, 616, and 633 keV. Band 4 also has two separate decay paths to band 6: a 924-keV transition to the yrast 8^+ state, and an 1144-keV transition to the yrast 6^+ state. These links, whose angular-intensity ratios are reported in Table III, have been assigned to be $I \rightarrow I$ transitions in order to ensure experimentally reasonable multipolarities for the transitions connecting bands 3 and 4. Even spins are established for band 4 as a result of these assignments, and systematic behavior suggests that the band most likely has negative parity.

Both bands 9 and 11 decay to band 10 at low spins. No new links between band 10 and the yrast positive-parity cascade have been found, but several new decay paths which separately connect bands 9 and 11 to yrast states in band 6 have been observed. Spin and parity assignments to band 11 are based upon angular-intensity ratios extracted for the 1112-keV link to the yrast $I^\pi = 4^+$ state; these ratios are suggestive of a $\Delta I = 1$ mixed $M1/E2$ multipolarity, implying odd spins and even parity for the band. Five new transitions

have been added to band 11, and a single new transition has been added to band 9.

The band labeled 1 in Fig. 2 consists of two cascades of $\Delta I = 2$ transitions connected by a series of $\Delta I = 1$ transitions. Though this band could not be extended in the present work, additional decay paths have been identified which firmly establish the spins and parities of the low-lying $I^\pi = 7^-$ and 8^- states. The level populated by the 419-keV transition in this band decays by a 1233-keV transition to the yrast 6^+ state and also by a very weak 635-keV transition to the 5^- state in band 3. Angular-correlation analysis suggests that the former link has an $E1$ multipolarity. Given this information and the observed decay pattern, the spin and parity of this level have been assigned to be 7^-. Establishing the spin and parity of the 8^- state follows from a complete consideration of all available information. To begin, an 1133-keV transition connects the state populated by the 515-keV transition to the yrast 8^+ level; angular-intensity ratios measured for this link are consistent with a pure, stretched-dipole character, thus yielding an $I^\pi = 9^-$ assignment, in agreement with earlier findings. Angular-correlation analysis also indicates that the 247-keV transition interlinking the two $\Delta I = 2$ cascades has $\Delta I = 1$ mixed $M1/E2$ multipolarity. This determines the spin and parity assignment to the 10^- state. Finally, the ratios R_{DCO} extracted for the 404- and 419-keV transitions within band 1 support assigning the former transition as a stretched electric quadrupole and the latter as a $\Delta I = 1$ mixed $M1/E2$ dipole, thus generating the spin and parity assignment to the 8^- state.

As indicated in Fig. 2, the $I^\pi = 10^-$ state in band 1 has several alternate decay paths through an intermediate level labeled X for clarity. The 10^- state decays to this level by a 192-keV transition whose measured angular-intensity ratio R'_{DCO} supports a $\Delta I = 1$ mixed $M1/E2$ multipolarity assignment. Taken together, this ratio and the decay pattern of the intermediate level suggest a spin and parity assignment of 9^-.

The new band labeled 2 in Fig. 2 consists of five levels; this band feeds the state labeled X by a 578-keV transition. Although this band also decays to band 3 by a 298-keV transition, neither linking transition was sufficiently intense to permit angular-correlation analysis. Tentative spin and parity assignments have been determined for this band on the basis of yrast arguments and decay considerations.

IV. DISCUSSION

As suggested above, the level schemes extracted for ^{116}Xe and ^{118}Xe are quite complex. While these nuclei do indeed manifest a number of different structures, they also share several related features since, as isotopes, they have similar proton Fermi surfaces. Interpretations of several of these features in ^{118}Xe were given in Ref. [23]. Accordingly, this discussion will focus on ^{116}Xe and those bands identified for the first time in ^{118}Xe. The discussion itself has been organized into two parts which separately address positive- and negative-parity bands. Within each part, related bands in both isotopes are discussed together so as to exploit systematic behaviors. A brief listing of the configuration assignments proposed in this discussion for the bands observed in ^{116}Xe and ^{118}Xe can be found in Table VI.

TABLE VI. Configuration assignments proposed for bands observed in ^{116}Xe and ^{118}Xe. Bands are referred to by their numbered labels shown in Figs. 1 and 2, respectively. See Sec. IV for discussion.

Bands in ^{116}Xe	Bands in ^{118}Xe	Configuration assignment
2	10	even-spin quasirotational γ band
	11	odd-spin quasirotational γ band
	11 [a]	odd-spin quasirotational γ band $\otimes$ aligned $(\nu h_{11/2})^2$ configuration
	7	even-spin quasirotational γ band $\otimes$ aligned $(\nu h_{11/2})^2$ configuration
4	6	ground-state band
4 [a]	6 [a]	ground-state band $\otimes$ aligned $(\pi h_{11/2})^2$ configuration
3	9	ground-state band $\otimes$ aligned $(\nu h_{11/2})^2$ configuration
4 [b]		aligned $(\pi h_{11/2})^2$ band $\otimes$ aligned $(\nu h_{11/2})^2$ configuration
8	3	favored signature $\pi[h_{11/2}g_{7/2}]$
7 [c]	4	unfavored signature $\pi[h_{11/2}g_{7/2}]$
7 [c]		favored signature $\pi[h_{11/2}d_{5/2}]$
6		$\nu[h_{11/2}(g_{7/2},d_{5/2})^1]$
	1	$\pi[(g_{9/2})^{-1}h_{11/2}]$
5		$\pi[h_{11/2}(g_{7/2},d_{5/2})^3]\otimes\nu[(h_{11/2})^3(g_{7/2},d_{5/2})^9]$

[a]Crossing occurs at frequencies $\omega\approx\omega_1$.

[b]Crossing occurs at frequencies $\omega\approx\omega_2$.

[c]Two alternate interpretations are proposed.

A. Positive-parity bands

1. ^{116}Xe, band 4, and ^{118}Xe, bands 6 and 8

Experimental alignments i_x extracted for the yrast positive-parity bands in ^{116}Xe and ^{118}Xe are displayed in Fig. 9 as a function of rotational frequency. As can be seen in the figure, the yrast band in ^{116}Xe shows two gradual gains in alignment at $\omega_1=0.39$ MeV/$\hbar$ and $\omega_2=0.51$ MeV/$\hbar$, and also a small increase at $\omega_4\approx0.74$ MeV/$\hbar$. In contrast, the yrast band in ^{118}Xe shows only two sharp gains in alignment, the first occurring at the same frequency as that in ^{116}Xe and the second at $\omega_3\approx0.64$ MeV/$\hbar$. A discussion of these alignments is presented below within the context of systematic behaviors identified in heavier even xenon isotopes.

The yrast positive-parity bands in the heavier even $^{120-126}$Xe isotopes all show an alignment at $\omega_1\approx0.39$ MeV/$\hbar$, proceeding from an upbend in ^{120}Xe to a backbend in ^{126}Xe (see, for example, Ref. [23]). In the $A\geq122$ Xe isotopes, these alignments have been attributed to pairs of $h_{11/2}$ neutrons. However, as pointed out in Ref. [23], additional aligned angular momentum is gained in the cases of ^{118}Xe and ^{120}Xe, which suggests different aligning particles for the lighter and heavier Xe isotopes.

Two different interpretations have been proposed in Refs. [14] and [23] for the alignment observed at ω_1 in ^{118}Xe. In Ref. [23], the alignment behaviors of ^{118}Xe and ^{120}Xe were compared to those of the $Z=56$ isotones ^{120}Ba and ^{122}Ba, respectively. As shown in Fig. 10(a) of that reference, similar upbends were observed to occur in the alignment patterns of these four nuclides at frequencies near ω_1. In the ^{120,122}Ba isotopes, these upbends were attributed [31,32] to the near superposition of closely spaced $h_{11/2}$ proton and $h_{11/2}$ neutron

alignments. Given this understanding, an interpretation involving nearly simultaneous $h_{11/2}$ proton and $h_{11/2}$ neutron alignments was proposed in Ref. [23] for the upbends observed in the ^{118,120}Xe isotopes. In the interpretation proposed in Ref. [14], however, the upbend in ^{118}Xe was attributed solely to $h_{11/2}$ protons on the basis of blocking
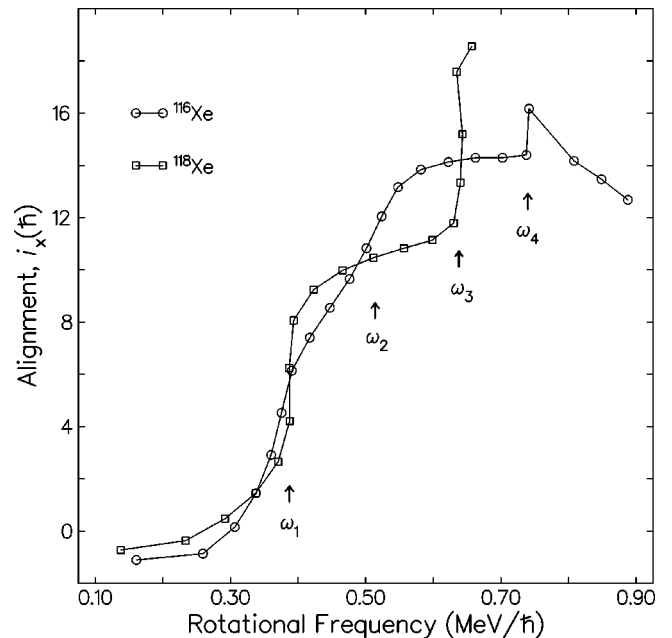
FIG. 9. Experimental alignments i_x for the yrast positive-parity bands in ^{116}Xe and ^{118}Xe calculated relative to a frequency-dependent moment of inertia reference described by the Harris parameters used in Ref. [23], $\mathcal{J}_0=15\ \hbar^2/$MeV and $\mathcal{J}_1=25\ \hbar^4/$MeV^3.
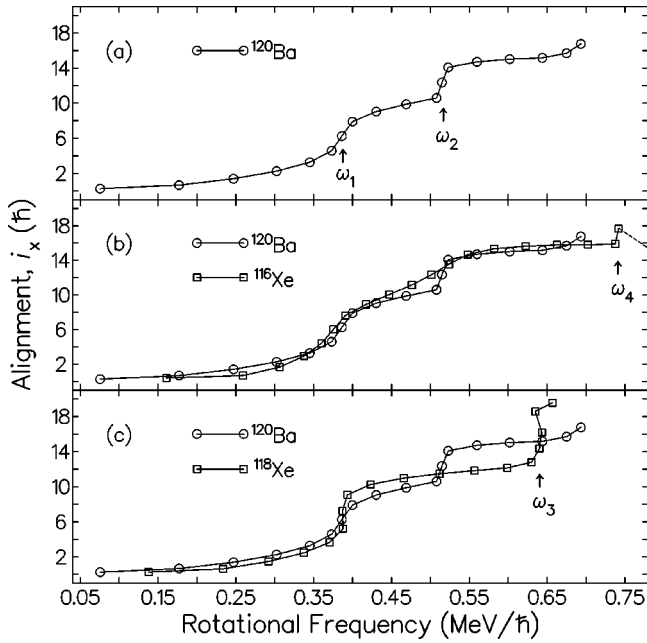
FIG. 10. Experimental alignment i_x extracted for the yrast positive-parity band in ^{120}Ba (a) compared to the alignment for the yrast positive-parity band in ^{116}Xe ($+1.5\hbar$) (b) and ^{118}Xe ($+1.0\hbar$) (c). Alignments have been calculated using the Harris parameters indicated in the caption to Fig. 9.

arguments with the $\nu h_{11/2}$ and $\pi h_{11/2}$ yrast bands in the nearby odd-neutron ^{117}Xe and odd-proton ^{117}I nuclides, respectively.

A conclusive distinction can be made between these alternate interpretations by referring to recent experimental data for ^{120}Ba, in which the yrast positive-parity band has been extended to $36\hbar$ [33]. The experimental alignment extracted for this band is shown here in Fig. 10(a). As seen in this figure, two distinct upbends are now observed in ^{120}Ba, the first at $\omega_1 \approx 0.36$ MeV/$\hbar$ and the second at $\omega_2 \approx 0.52$ MeV/$\hbar$. These upbends have been interpreted by comparing the alignment behavior in ^{120}Ba to that extracted for the $\nu g_{7/2}$ and $\nu h_{11/2}$ bands in the odd-mass ^{119}Ba isotope; these latter two bands have been extended also in recent experimental data [33]. On the basis of this comparison, the first (second) alignment in ^{120}Ba has been attributed solely to $h_{11/2}$ protons ($h_{11/2}$ neutrons) [33]. The alignments for ^{116}Xe and ^{118}Xe are compared to ^{120}Ba in Figs. 10(b) and 10(c), respectively; in these figures, $1.5\hbar$ ($1.0\hbar$) has been added to the alignment values for ^{116}Xe (^{118}Xe) for purposes of comparison. (While the level scheme for ^{118}Ba, the $Z=56$ isotone of ^{116}Xe, has been established recently [34], the yrast band has not been followed through the first alignment, thus precluding a meaningful comparison with ^{116}Xe.) Similar to Fig. 10(a) in Ref. [23], Figs. 10(b) and 10(c) demonstrate that the alignment behaviors of the yrast bands in ^{116}Xe, ^{118}Xe, and ^{120}Ba are all quite similar in the vicinity of the upbends at ω_1. Given the current interpretation of ^{120}Ba, the alignments at ω_1 in ^{116}Xe and ^{118}Xe are assigned here to be due solely to $h_{11/2}$ protons; equivalently stated, the ground-state bands in these isotopes are understood to be crossed at ω_1 by aligned two-quasiparticle $(\pi h_{11/2})^2$ configurations, thereby generating yrast-aligned $(\pi h_{11/2})^2$ bands. This ex-

planation is consistent with Ref. [14] and the blocking arguments presented therein.

Further comparison of the alignment behaviors observed in ^{116}Xe and ^{120}Ba proves helpful to understanding the nature of the second alignment in ^{116}Xe even though these nuclides are not isotones. As shown in Fig. 10(b), the yrast bands in ^{116}Xe and ^{120}Ba both experience upbends at $\omega_2 \approx 0.52$ MeV/$\hbar$. In addition, the total amounts of aligned angular momenta generated just after these upbends are virtually identical. Such close agreement suggests that the second alignments in ^{116}Xe and ^{120}Ba have similar origins. Accordingly, the alignment observed at ω_2 in ^{116}Xe is assigned here to be due to $h_{11/2}$ neutrons; equivalently stated, the aligned $(\pi h_{11/2})^2$ band in ^{116}Xe is understood to be crossed at ω_2 by the aligned two-quasiparticle $(\nu h_{11/2})^2$ configuration, thereby generating an yrast-aligned $(\pi h_{11/2})^2 \otimes (\nu h_{11/2})^2$ band. This explanation is also consistent with Ref. [14] and the blocking arguments in ^{117}Xe and ^{117}I discussed therein.

Just as for the upbend at ω_1, two different explanations have been proposed for the sharp alignment gain observed at ω_3 in ^{118}Xe. This feature was understood initially in Ref. [23] to be evidence for the interruption of the band by an aligned single-particle state, and interpreted later in Ref. [14] to be the result of a normal pair alignment. As discussed in Sec. III above, the yrast band for ^{118}Xe presented in Ref. [14] has been revised substantially in the present work. Because of this revision, we find better agreement with the interpretation proposed in Ref. [23]. The sharp alignment at ω_3 arises directly from the bunching together of four γ-ray transitions in the yrast band at energies $E_\gamma \sim 1270$ keV. Results of calculations based on the total Routhian surface (TRS) formalism [35–37] reported in Ref. [23] for ^{118}Xe predict that a state based on the $\pi[(h_{11/2})^2(g_{7/2},d_{5/2})^2]_{16^+} \otimes \nu[(h_{11/2})^4(g_{7/2},d_{5/2})^{10}]_{20^+}$ single-particle configuration will interrupt the collective rotational states at $I^\pi = 36^+$. (This is not a predicted smooth-termination state; see below.) Although a 36^+ state was not observed in Ref. [23], the present spectrum of the yrast band does support the assignment of the yrast (36^+) state to this single-particle configuration. Near this state, the yrast band fragments into several γ-ray transitions, resulting in a sharp decline in intraband intensity. Both of these features are associated with the interruption of a collective rotational band by an aligned single-particle state. This interpretation suggests that a second alignment arising from a pair of $h_{11/2}$ neutrons has not been observed in the yrast band in ^{118}Xe. Considering the understanding of the second alignments in the yrast bands of both ^{116}Xe and ^{120}Ba, this is an unexpected result, and may be caused by the apparent interruption of the band occurring at the (36^+) state.

As alluded to above, the aligned single-particle state which appears to be interrupting the yrast band in ^{118}Xe is not a predicted smooth-termination state. Assuming the alignment of all valence nucleons consistent with the Pauli principle, the $\pi[(h_{11/2})^2(g_{7/2},d_{5/2})^2] \otimes \nu[(h_{11/2})^4(g_{7/2},d_{5/2})^{10}]$ configuration has a maximum spin of $42\hbar$. If the yrast band were built on this configuration, the band would be expected to terminate at spin 42, in disagreement with experimental observations. Theoretical calculations as discussed below for band 5 in ^{116}Xe suggest that the

yrast band in ^{118}Xe, as well as the yrast band in ^{116}Xe, can be attributed to a configuration of the form [02,4] in the notation of Sec. IV A 4. In ^{118}Xe, this configuration includes ten valence neutrons which are distributed over the positive-parity $g_{7/2}$, $d_{5/2}$, $d_{3/2}$, and $s_{1/2}$ orbitals. Calculations indicate that the most energetically favored configuration of this form includes eight neutrons in the $g_{7/2}, d_{5/2}$ orbitals and two neutrons in the $d_{3/2}, s_{1/2}$ orbitals. Since such a [02,4] configuration has a maximum spin of $48\hbar$, the yrast band in ^{118}Xe does not appear to have been observed to the predicted smooth-termination state. (Theoretical calculations shown in Fig. 13 suggest that the yrast band in ^{116}Xe has been observed to within two transitions of the smooth-termination state predicted at $46\hbar$ for the corresponding [02,4] configuration.)

Band 8 in ^{118}Xe has been observed to decay into band 6 near the $I^\pi = (26^+)$ state. As described earlier, many of the γ-ray transitions identified in this band had been assigned most recently to band 6, thereby generating a maximum observed spin in the yrast band of (46^+) [14]. Prior to the present work, Ragnarsson and Afanasjev reported the results of calculations for ^{118}Xe which were performed in order to examine configurations which terminate in the available valence space [24]. These calculations were not able to reproduce the very low cost in energy of spin units above $I \approx 40\hbar$ in the experimental spectrum of the yrast band reported in Ref. [14]. This disagreement has been resolved now by the experimental observation of the parallel band 8, which implies a yrast band much less extended in spin than previously thought [38]. At present, the interpretation of this sideband remains unclear. In ^{116}Xe, a two-level sequence with a similar decay pattern has been identified at much higher spins. Judging by the crossing frequency with the yrast band, this sequence may be related to the nearby alignment gain observed at ω_4. [Note that ^{120}Ba also appears to experience a third alignment gain at high frequency; see Fig. 10(a).] Currently, these unusual features in ^{116}Xe and ^{118}Xe are the subject of theoretical investigations [38].

2. ^{116}Xe, bands 2 and 3, and ^{118}Xe, bands 9 and 10

Considered as pairs, band 2 (3) in ^{116}Xe and band 10 (9) in ^{118}Xe share many features. Bands 2 and 10 originate at low excitation energies, have similar decay patterns, and have been interpreted in both Xe isotopes as even-spin quasirotational γ bands [39,40]. These bands are crossed by bands 3 and 9 at frequencies near 0.31 MeV/$\hbar$. Bands 3 and 9 themselves also have similar decay patterns, and cross the extrapolated yrast bands at frequencies near 0.41 MeV/$\hbar$. Experimental alignments i_x extracted for bands 3 and 9 are shown in Figs. 11(a) and 11(b), respectively, where the alignments of the yrast bands at low frequencies are presented for comparison. These figures demonstrate that the amounts of aligned angular momenta in bands 3 and 9 are near $7\hbar$ initially, and then gradually increase with increasing rotational frequency.

As discussed in the previous section, the ground-state bands in ^{116}Xe and ^{118}Xe have been understood to be crossed at ω_1 by aligned two-quasiparticle $(\pi h_{11/2})^2$ configurations, thereby generating yrast-aligned $(\pi h_{11/2})^2$ bands. Since systematic behavior [41] suggests that the
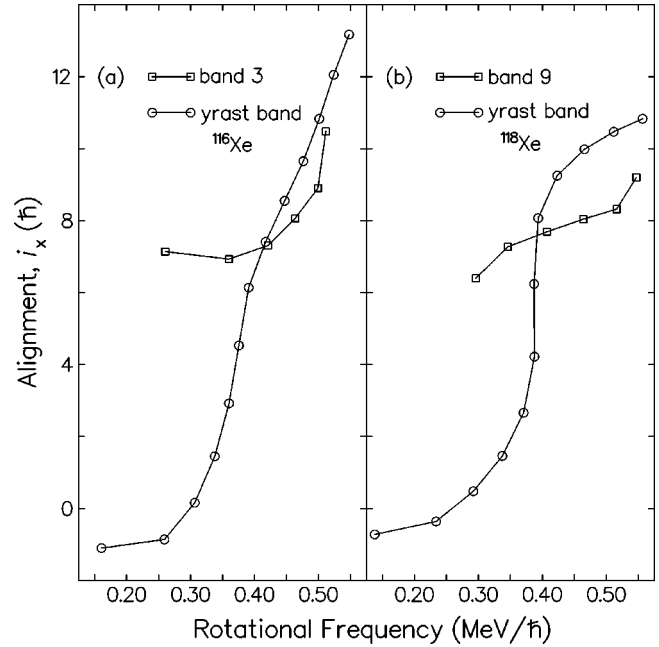
FIG. 11. Experimental alignments i_x for band 3 in ^{116}Xe (a) and band 9 in ^{118}Xe (b) calculated using the Harris parameters indicated in the caption to Fig. 9. Alignments of the yrast bands in ^{116}Xe (a) and ^{118}Xe (b) at low frequencies are shown for comparison.

ground-state bands also will be crossed at frequencies near ω_1 by aligned two-quasiparticle $(\nu h_{11/2})^2$ configurations, aligned $(\nu h_{11/2})^2$ bands are expected to coexist with the observed $(\pi h_{11/2})^2$ bands at low excitation energies.

In Ref. [23], band 9 in ^{118}Xe was assigned to be an aligned two-quasiparticle $(\nu h_{11/2})^2$ band on the basis of the observed alignment pattern and extracted crossing frequencies. The close similarities between this band 9 and band 3 in ^{116}Xe, as described above, suggest that band 3 also may be so identified. Like band 9, the initial amount of aligned angular momenta in band 3 resembles that in the aligned $(\nu h_{11/2})^2$ bands in the heavier $A \geqslant 122$ Xe isotopes. Moreover, the extrapolated crossing frequency with the yrast band, slightly greater than $\omega_1 = 0.39$ MeV/$\hbar$, is consistent with the systematics presented in Ref. [41] for the crossing frequencies of aligned two-quasiparticle $(\nu h_{11/2})^2$ configurations. Given these considerations, band 3 in ^{116}Xe can be assigned reasonably as an aligned $(\nu h_{11/2})^2$ band. The aligned $(\nu h_{11/2})^2$ configuration has a preferred negative γ deformation. As mentioned in Ref. [23] for bands 9 and 10 in ^{118}Xe, such a deformation might lead to a large overlap with the quasirotational γ band, and could account for the low crossing frequency of bands 3 and 2 in ^{116}Xe.

3. ^{118}Xe, bands 7 and 11

Band 11 in ^{118}Xe includes nine levels and has been followed up to a level spin of $I^\pi = (19^+)$. At low spin, this band has been interpreted to be the odd-spin analog of band 10 in ^{118}Xe [40]. A similarly understood odd-spin band was reported in ^{116}Xe in Ref. [39], but could not be confirmed in the present work.

The experimental alignment i_x extracted for band 11 in ^{118}Xe is shown in Fig. 12, where the alignment of the yrast band at low frequencies is presented for comparison. As demonstrated in the figure, both the yrast band and band 11
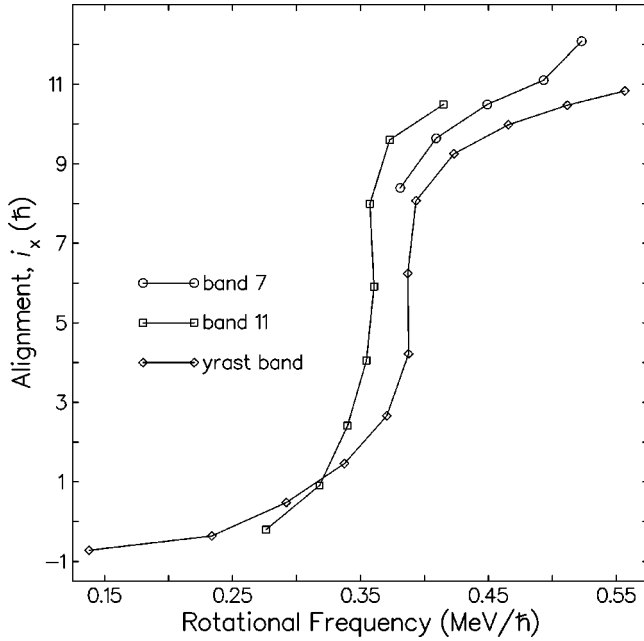
FIG. 12. Experimental alignments i_x for bands 7 and 11 in ^{118}Xe calculated using the Harris parameters indicated in the caption to Fig. 9. The alignment of the yrast band in ^{118}Xe at low frequencies has been shown for comparison.

in ^{118}Xe experience similar alignment gains at $\omega_1 \approx 0.39$ MeV/$\hbar$. Despite this close resemblence, the upbend occurring near ω_1 in band 11 does not appear to be due to $h_{11/2}$ protons, as in the yrast band, but to $h_{11/2}$ neutrons. As discussed above, aligned two-quasiparticle $(\pi h_{11/2})^2$ and $(\nu h_{11/2})^2$ configurations both cross the ground-state band in ^{118}Xe at similar frequencies. If band 11 were like the ground-state band, these configurations could be expected to cross band 11 at similar frequencies also. Band 11, however, is a quasirotational γ band at low spin, and, unlike the ground-state band, has varying γ deformations; such deformations would enhance the likelihood of the rotational alignment of a pair of $h_{11/2}$ neutrons over $h_{11/2}$ protons. Given this consideration, the upbend observed at ω_1 in band 11 is attributed here to $h_{11/2}$ neutrons. This interpretation appears to be consistent with the crossing frequency and alignment gain shown in Fig. 12.

Band 7 in ^{118}Xe consists of six levels and has been followed up to a level spin of $I^\pi = (24^+)$. Relevant features concerning the origin of this band can be deduced by comparing the behavior of band 7 to that of band 9. As mentioned earlier, band 9 decays to the yrast band primarily by low-energy transitions having dominant $I \rightarrow I$ $M1$ character. The only pure stretched-quadrupole transition observed in the decay path to the yrast band originates from the 10^+ bandhead and does not compete with the much more intense $I \rightarrow I$ $M1$ transition. In contrast, the decay path of band 7 includes several pure stretched quadrupoles which are competitive with the $I \rightarrow I$ $M1$ transitions. The experimental alignment extracted for band 7 is shown in Fig. 12, where the alignments of the yrast band and band 11 also are presented. As displayed in the figure, the alignment in band 7 follows the patterns in these two bands closely, beginning at $8\hbar$ and upbending at a frequency near 0.40 MeV/$\hbar$. This behavior differs markedly with that of the alignment in band 9, which

neither upbends nor follows the pattern of the yrast band [see Fig. 11(b)].

The differences just described between bands 7 and 9 strongly suggest that these bands do not both result from crossings of the ground-state band by aligned two-quasiparticle configurations. A band with a behavior similar to that of band 7 has been observed in ^{120}Xe, however, where extracted ratios of reduced transition probabilities $B(E2; I \rightarrow I-2; \text{interband})/B(E2; I \rightarrow I-2; \text{intraband}) \approx 0.1$ were understood as evidence for a quasirotational γ band coupled to an aligned two-quasiparticle configuration [23]. Given the description above, band 7 appears to be consistent with this explanation, though the $B(E2; \text{out})/B(E2; \text{in})$ ratios extracted for decays from the $I^\pi = (16^+)$ and (18^+) states are smaller (about 0.04 and 0.02, respectively). The close correspondence between the alignments of bands 7 and 11 suggests that these bands are related. As discussed earlier, band 11 can be understood at high frequencies to be an odd-spin quasirotational γ band coupled to the aligned $(\nu h_{11/2})^2$ configuration. Since the initial alignment of $8\hbar$ in band 7 suggests that the crossing of the two-quasiparticle configuration likely has already occurred, band 7 can be assigned reasonably as the even-spin analog (i.e., "signature partner") to band 11.

4. ^{116}Xe, band 5, and ^{118}Xe, band 5

As noted earlier, neither band 5 in ^{116}Xe nor band 5 in ^{118}Xe could be linked conclusively to known low-lying states. Tentative spin and parity assignments have been determined for these bands on the basis of yrast arguments and decay considerations. The discussion below proceeds assuming this tentative character.

Band 5 in ^{116}Xe includes nine levels and has been followed up to a rotational frequency in excess of 0.90 MeV/$\hbar$. As shown in the spectrum of Fig. 4, this band manifests an increase in the energy spacings between adjacent γ-ray transitions with increasing transition energy. This observation suggests that band 5 may be described within the framework of smooth band termination [12,13].

Smooth band termination is a form of collective rotational behavior in which the nuclear shape gradually evolves over many γ-ray transitions from collective near-prolate ($\gamma \sim 0°$) to noncollective oblate ($\gamma = +60°$) as the Coriolis interaction aligns the valence particles and holes with the nuclear rotational axis. After the available valence particles and holes have aligned, the rotational band terminates at an angular momentum that exhausts the sum of the aligned single-particle spins.

Rotational bands in the Sb region [1–4,7,8,10] which have been understood within the framework of smooth band termination share several experimental features. One characteristic feature is a decreasing dynamic moment of inertia $\mathcal{J}^{(2)}$ with increasing rotational frequency, to values that are a fraction of the rigid-body estimates close to termination. This decrease appears to be associated with the increasing cost in energy to build higher units of angular momentum as the nucleus approaches the noncollective oblate shape [13]. Another related feature is a substantial difference between the dynamic $\mathcal{J}^{(2)}$ and kinematic $\mathcal{J}^{(1)}$ moments of inertia at frequencies near termination, such that $\mathcal{J}^{(2)} < \mathcal{J}^{(1)}$. As shown in Fig. 5, band 5 in ^{116}Xe also shares these two features;
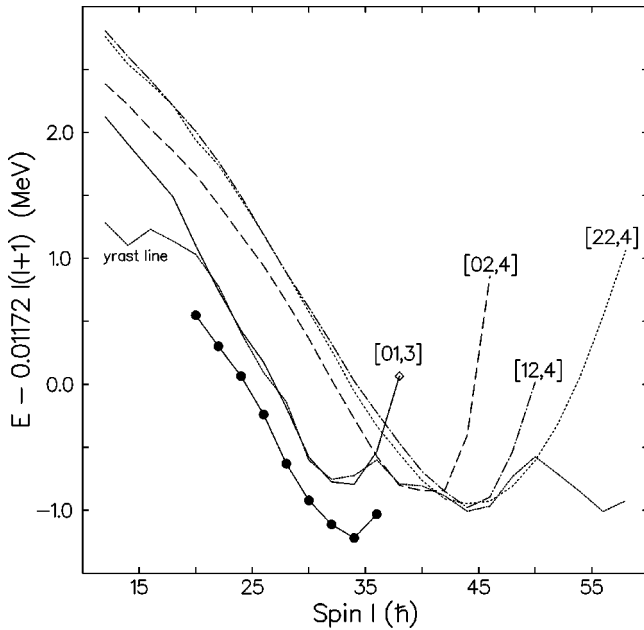
FIG. 13. Rigid-rotor plot of band 5 in ^{116}Xe and calculated yrast configurations having parity and signature (+,0). Experimental values are indicated by solid symbols and theoretical results by labeled curves. A dotted line represents the calculated yrast line for the stated parity and signature combination, and an open diamond denotes the predicted smooth termination state of the [01,3] configuration.

these experimental observations are interpreted as evidence for smooth band termination.

Theoretical calculations also have been undertaken [38] within the configuration-dependent shell-correction approach [42] to explore the termination properties of band 5 in ^{116}Xe and identify its microscopic configuration. The energy in these calculations is minimized with respect to the deformation parameters (ε_2, ε_4, γ) by using a cranked Nilsson potential to describe the rotating mean field and performing shell corrections according to the Strutinsky prescription. Pairing correlations have been neglected, and specific techniques explained in Ref. [13] for orbital tracing have been employed. Individual configurations can be followed in calculations over a large spin range, up to the maximum spins for band termination. In this section, configurations relative to the doubly magic ^{100}Sn core will be labeled using the shorthand notation $[p_1 p_2, n]$, in which p_1, p_2, and n are the numbers of proton holes in the $g_{9/2}$ orbital, of protons in the $h_{11/2}$ orbital, and of neutrons in the $h_{11/2}$ orbital, respectively [13].

These calculations have identified the configuration responsible for band 5 in ^{116}Xe to be [01,3], which can be written as $\pi[h_{11/2}(g_{7/2},d_{5/2})^3] \otimes \nu[(h_{11/2})^3(g_{7/2},d_{5/2})^9]$ relative to the $Z=N=50$ doubly closed shell. A comparison between the energies of band 5 and the [01,3] configuration calculated relative to a rigid-rotor reference is presented as a function of spin in Fig. 13. For purposes of comparison, the experimental curve in this figure has been offset by an arbitrary amount from the calculated curves since the absolute energy of band 5 is unknown. Figure 13 shows that calculations for the [01,3] configuration reproduce the general shape and minimum of the experimental curve rather well. Assum-

ing an alignment of all particles consistent with the Pauli principle, the $\pi[h_{11/2}(g_{7/2},d_{5/2})^3] \otimes \nu[(h_{11/2})^3(g_{7/2},d_{5/2})^9]$ configuration has a maximum spin of $38\hbar$, hinting that band 5 may have been observed to the penultimate state ($\pm 2\hbar$ experimental uncertainty) before predicted smooth termination. Given the available experimental evidence, the assignment of band 5 in ^{116}Xe to the [01,3] configuration represents a probable interpretation.

Band 5 in ^{118}Xe includes seven levels and has been followed up to a rotational frequency near 0.60 MeV/$\hbar$. Unlike band 5 in ^{116}Xe, this band has not been observed significantly beyond the frequency regime where pairing correlations are known to be important ($I \lesssim 20\hbar$); consequently, theoretical calculations as discussed above will not be conclusive here. A comparison of the dynamic moments of inertia $\mathcal{J}^{(2)}$ extracted for these two bands does nonetheless provide information relevant to understanding the structure of band 5 in ^{118}Xe. These moments of inertia, shown in Figs. 5 and 8, manifest pronounced peaks at frequencies near 0.48 MeV/$\hbar$, suggesting related quasiparticle alignments. In the proposed explanation for band 5 in ^{116}Xe, this alignment would be consistent with the second crossing of a pair of $h_{11/2}$ neutrons, since the first crossing would be blocked by occupation of the $\nu h_{11/2}$ orbital. If this alignment does arise from the second $\nu h_{11/2}$ crossing, then the configuration responsible for band 5 in ^{118}Xe has an odd (>1) number of $h_{11/2}$ neutrons. With this consideration, two conclusions concerning the proton contribution to the responsible configuration are evident. If band 5 has positive parity, as suggested experimentally, then the proton contribution would include an odd number of $h_{11/2}$ orbitals; if band 5 has negative parity, contrary to experimental expectations, then the proton contribution would have positive parity. A further understanding of the configuration responsible for band 5 is not possible without rigorous spin and parity assignments.

As indicated in Sec. I above, the present work has been motivated by our observation of well-developed intruder rotational bands in the ^{114}Te [7] and ^{116}Te [8] isotopes, which are the corresponding $Z=52$ isotones of ^{116}Xe and ^{118}Xe. The yrast intruder bands in these two Te isotopes were interpreted within the framework of smooth band termination. On the basis of theoretical calculations like those described here, these bands were attributed to deformed $4p2h$ proton configurations involving $2p$-$2h$ proton excitations across the $Z=50$ shell gap. Intruder bands similarly attributed to deformed $5p2h$ proton configurations have been observed in both the ^{113}I [10] and ^{115}I [11] isotopes, the latter of which is the $Z=53$ isotone of ^{116}Xe. These observations suggest that intruder rotational bands built upon related deformed $6p2h$ proton configurations can be expected in ^{116}Xe and ^{118}Xe. Contrary to expectations, however, band 5 in ^{116}Xe, the only candidate for smooth band termination in these two Xe isotopes, appears to be built upon the [01,3] configuration, which does not involve any p-h proton excitations.

This unexpected result may be explained by the theoretical calculations shown in Fig. 13. As indicated in this figure, configurations in ^{116}Xe which are built upon deformed p-h proton excitations, such as the [12,4] and [22,4] configurations, are not predicted to approach the yrast line until very high spins $I \sim 45\hbar$; these spins are beyond the limit of ex-
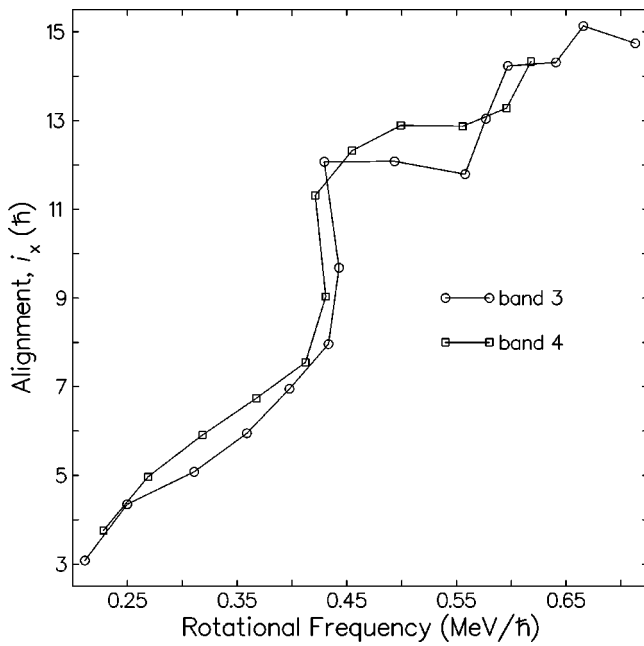
FIG. 14. Experimental alignments i_x for bands 3 and 4 in ^{118}Xe calculated using the Harris parameters indicated in the caption to Fig. 9.

FIG. 15. Experimental alignments i_x for bands 7 and 8 in ^{116}Xe calculated using the Harris parameters indicated in the caption to Fig. 9.

perimental sensitivity in the present work. Such a situation contrasts markedly with the light Te isotopes, where configurations involving deformed p-h proton excitations approach the yrast line in theoretical calculations at relatively low spins $I \sim 30\hbar$ (see Figs. 7 and 11 in Ref. [8]). These calculations imply that the available valence nucleons in the light $_{54}$Xe isotopes, unlike those in the light $_{52}$Te isotopes, are able to generate large amounts of collective angular momenta near the yrast line.

B. Negative-parity bands

1. ^{116}Xe, bands 7 and 8 and ^{118}Xe, bands 3 and 4

Bands 3 and 4 in ^{118}Xe have been extended [23] in this work by three and four transitions to level spins of $I^\pi = (35^-)$ and (30^-), respectively. The alignment patterns extracted for these low-lying, decoupled $(\Delta I = 2)$, negative-parity bands are shown in Fig. 14. As noted in Ref. [23], these bands have very similar alignment behaviors. Both bands experience gradual increases in alignment up to frequencies near 0.40 MeV/$\hbar$ and then sharp alignment gains of $4\hbar$ at approximately 0.44 MeV/$\hbar$. Additional sharp alignment gains also appear to occur in both bands at frequencies between 0.55 and 0.60 MeV/$\hbar$. While bands 3 and 4 each decay to band 6, the yrast positive-parity band, by electric dipole transitions, band 4 also connects to band 3 by several mixed $\Delta I = 1$ $M1/E2$ transitions. These weak linking transitions and the similar alignment behaviors shown in Fig. 14 suggest that bands 3 and 4 are signature partners.

For deformed prolate shapes in the ^{116}Xe and ^{118}Xe isotopes, the proton Fermi surface lies just below the low-Ω $h_{11/2}$ orbitals, and the neutron Fermi surface lies in the middle of the $h_{11/2}$ subshell. As a consequence, negative-parity bands built on two-quasiproton and two-quasineutron $h_{11/2}g_{7/2}$ and $h_{11/2}d_{5/2}$ configurations can be expected to be
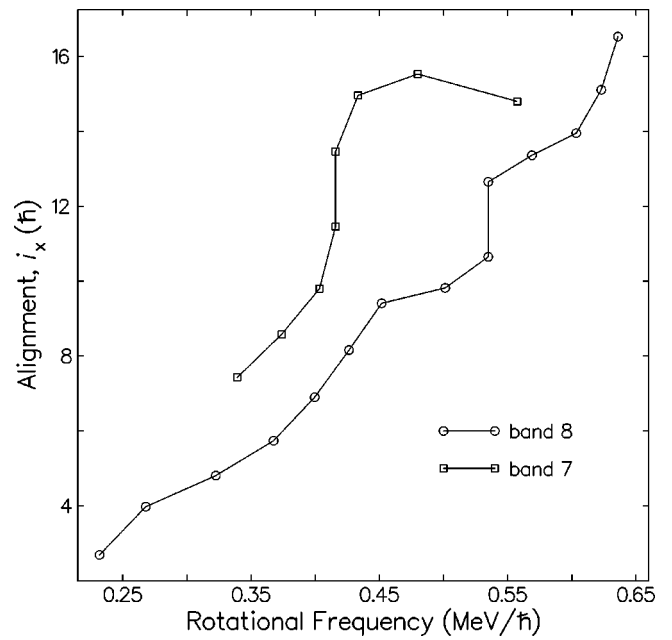
low lying. In Ref. [23], bands 3 and 4 in ^{118}Xe were noted to resemble the yrast negative-parity bands in neighboring Ba isotopes [31,32,43] at low spin. Given that these Ba bands were interpreted as having proton character, bands 3 and 4 in ^{118}Xe were understood in Ref. [23] as having proton character also, and were assigned to be signature partners based on the two-quasiproton $\pi[h_{11/2}g_{7/2}]$ configuration. This explanation agrees with the present data. The low K value of the $\pi[h_{11/2}g_{7/2}]$ configuration is consistent with the large signature splitting observed between bands 3 and 4 and also the fairly weak $\Delta I = 1$ $M1/E2$ crossovers, and the $\alpha = +1$ favored signature of the configuration is consistent with the odd-spin band 3 occurring at lower excitation energies than the even-spin band 4. As in Ref. [23], the sharp alignment gains identified at 0.44 MeV/$\hbar$ in these bands are attributed here to rotational alignments of pairs of $h_{11/2}$ neutrons. Two alternate explanations were proposed in Ref. [23] for the second sharp alignment gain in band 3, specifically, interruption of the band by an aligned single-particle state and the first nonblocked rotational alignment of a pair of $h_{11/2}$ protons. A second sharp alignment now also appears to occur in band 4 (see Fig. 14). The present development of bands 3 and 4 suggests that the gains in aligned angular momenta taking place near 0.60 MeV/$\hbar$ are the results of normal rotational alignments in a prolate nucleus; these upbends are attributed here to pairs of $h_{11/2}$ protons.

Band 8 in ^{116}Xe includes 15 levels and has been followed up to a level spin of $I^\pi = (33^-)$. The alignment pattern extracted for this low-lying, decoupled $(\Delta I = 2)$, negative-parity band is displayed in Fig. 15. As shown in this figure, the alignment behavior of band 8 resembles that observed in band 3 in ^{118}Xe; band 8 shows a gradual increase in alignment up to 0.40 MeV/$\hbar$. While band 8 does not experience a sharp alignment gain near 0.44 MeV/$\hbar$, the band does gain approximately $4\hbar$ in aligned angular momenta over the frequency range 0.45–0.55 MeV/$\hbar$. Moreover, band 8 appears
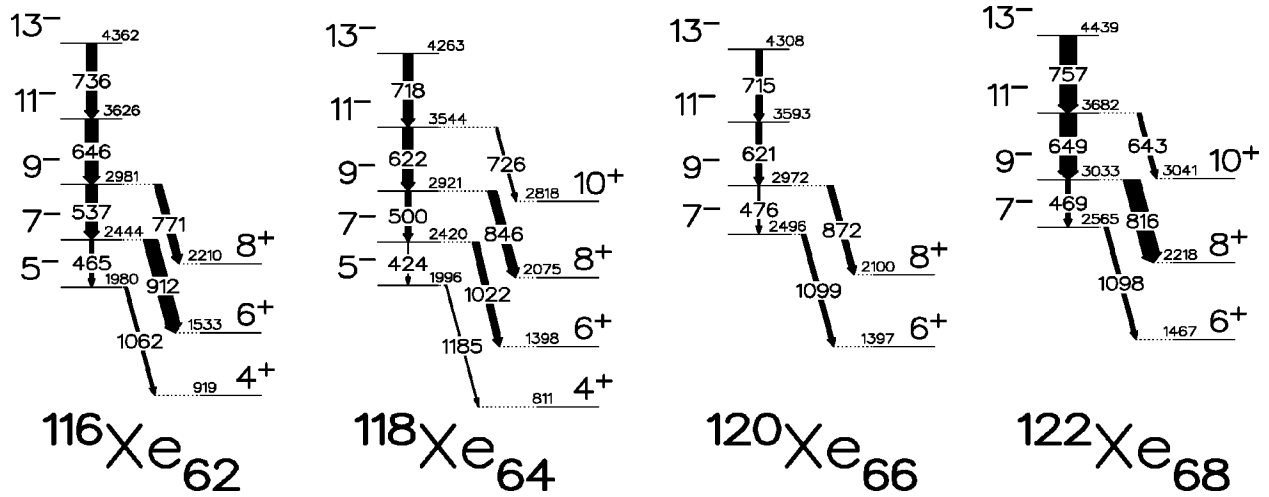
FIG. 16. Excitation energies and decay patterns of the first few states in band 8 in ^{116}Xe and the lowest odd-spin states in the $\pi[h_{11/2}g_{7/2}]$ bands in the even-mass $^{118-122}$Xe isotopes.

to undergo a second alignment gain near 0.60 MeV/$\hbar$. These similarities suggest that band 8 in ^{116}Xe and band 3 in ^{118}Xe are built on related configurations.

As already discussed, band 3 in ^{118}Xe has been attributed to the two-quasiproton $\pi[h_{11/2}g_{7/2}]$ configuration. In addition to ^{118}Xe, low-lying negative-parity bands generated by this same configuration have been observed in ^{120}Xe [23] and ^{122}Xe [44]. A comparison between the decay patterns and excitation energies of the lowest odd-spin states in these bands and the first few states in band 8 in ^{116}Xe is presented in Fig. 16. As shown in this figure (and also Fig. 1), band 8 decays to the yrast positive-parity band in ^{116}Xe by several intense electric dipole transitions. Figure 16 demonstrates that this decay pattern closely resembles that of the odd-spin $\pi[h_{11/2}g_{7/2}]$ bands in the heavier even-mass Xe isotopes. This figure also demonstrates that the excitation energies of the lowest negative-parity states in the even $^{116-122}$Xe nuclides follow a smooth systematic behavior. Given this trend, the similar decay patterns, and the alignment features described above, the assignment of band 8 in ^{116}Xe as the favored signature of the two-quasiproton $\pi[h_{11/2}g_{7/2}]$ configuration appears to be a plausible explanation. As in band 3 in ^{118}Xe, the first and second alignments in band 8 can be associated with pairs of $h_{11/2}$ neutrons and $h_{11/2}$ protons, respectively.

Band 7 in ^{116}Xe includes nine levels and has been followed up to a rotational frequency near 0.55 MeV/$\hbar$. While this band could not be linked definitively to known states in the ^{116}Xe level scheme, approximately 2/3 (1/3) of the band's intensity does appear to feed low-lying states in band 8 (6). An experimental alignment i_x has been extracted for band 7 assuming the tentative spin and parity assignments indicated in Fig. 1; this alignment is compared to that of band 8 in Fig. 15. As seen in this figure, band 7 undergoes an alignment gain of approximately $5\hbar$ at the frequency 0.42 MeV/$\hbar$.

While an exact understanding of band 7 cannot be determined without rigorous spin and parity assignments, four two-quasiparticle configurations are expected to generate low-lying negative-parity excitations in ^{116}Xe. As alluded to above, these are the two-quasiproton and two-quasineutron

$h_{11/2}g_{7/2}$ and $h_{11/2}d_{5/2}$ configurations. Two alternate explanations appear likely for band 7 given this consideration. As one possibility, band 7 could be the signature partner of band 8 in ^{116}Xe. Admittedly, the alignment patterns of these two bands are unusual for signature partners (see Fig. 15), but bands 7 and 8 do experience similar alignment gains at nearby frequencies. Since the $\pi[h_{11/2}g_{7/2}]$ configuration has a low K value, this explanation would be consistent with the failure to observe any $\Delta I = 1$ $M1/E2$ crossovers between the bands. As an alternative, band 7 could be the favored signature of the $\pi[h_{11/2}d_{5/2}]$ configuration. This configuration also has a low K value and, as such, would be consistent with the absence of an observed signature partner for band 7.

In both of the above explanations, the upbend identified at 0.42 MeV/$\hbar$ in the alignment curve for band 7 would arise from the rotational alignment of a pair of $h_{11/2}$ neutrons. The discussion of the yrast positive-parity band in ^{116}Xe (see earlier) indicates that pairs of $h_{11/2}$ protons are also expected to align at such low frequencies. Although both of the low-lying two-quasineutron $\nu[h_{11/2}g_{7/2}]$ and $\nu[h_{11/2}d_{5/2}]$ configurations could generate this proton alignment, neither of these configurations appears to be consistent with the present data for band 7. Unlike the two-quasiproton configurations, these two-quasineutron configurations have fairly high K values, and would thus be expected to produce strongly coupled bands with small signature splitting, in contrast with experimental observations. Accordingly, band 7 appears to be based on either the $\pi[h_{11/2}g_{7/2}]$ or $\pi[h_{11/2}d_{5/2}]$ two-quasiproton configuration.

As noted above, band 8 in ^{116}Xe and bands 3 and 4 in ^{118}Xe decay to the corresponding yrast positive-parity bands by electric dipole transitions. Reduced transition probabilities of $B(E1) \approx 2-4 \times 10^{-4}$ e^2 fm^2 have been calculated for these transitions using $B(E1)/B(E2)$ ratios extracted from the experimental data and quadrupole moments Q_0 estimated with techniques described in the next section. Specific $B(E1)$ values for individual linking transitions are listed in Table VII. These transition rates are comparable to those which have been extracted in ^{110}Te [45], ^{114}Xe [46], and ^{118}Ba [34] and understood as evidence for octupole correlations related to the $\nu h_{11/2}$ and $\nu d_{5/2}$ orbitals having Δj

TABLE VII. Reduced transition probabilities $B(E1)$ calculated for transitions in the decay paths of bands 6 and 8 in ^{116}Xe and bands 3 and 4 in ^{118}Xe.

Nucleus	Band	Q_0 (e b)	$I_i^\pi \rightarrow I_f^\pi$	$B(E1)$ (10^{-4} e^2 fm^2)
^{116}Xe	6	3.50	$8^- \rightarrow 8^+$	1.07 ± 0.10
	8	3.48	$7^- \rightarrow 6^+$	4.66 ± 0.21
			$9^- \rightarrow 8^+$	2.42 ± 0.13
^{118}Xe	3	3.55	$7^- \rightarrow 6^+$	3.50 ± 0.14
			$9^- \rightarrow 8^+$	3.42 ± 0.16
			$11^- \rightarrow 10^+$	1.79 ± 0.51
	4		$8^- \rightarrow 8^+$	1.69 ± 0.27

$=\Delta I=3$. Like the negative-parity bands in these particular nuclides, band 8 in ^{116}Xe and bands 3 and 4 in ^{118}Xe appear at fairly low excitation energies and have initial amounts of aligned angular momenta near $3\hbar$ (see Figs. 14, 15, and 16). These observations and the enhanced transition rates suggest that octupole correlations also may be involved at low spin in the decoupled negative-parity bands in ^{116}Xe and ^{118}Xe [23].

2. ^{116}Xe, band 6 and ^{118}Xe, band 1

Band 1 in ^{118}Xe, a strongly coupled ($\Delta I=1$) negative-parity band, has been followed to the $I^\pi=(19^-)$ state. No new transitions have been observed [23] in this band. Experimental Routhians e' extracted for the two opposite signatures of band 1 are displayed in Fig. 17(a). As shown in this figure, the Routhians of the $\alpha=0$ and $+1$ signatures are nearly degenerate over the entire range of observed frequencies.

Band 6 in ^{116}Xe, also a strongly coupled ($\Delta I=1$) negative-parity band, has been observed for the first time in the present work. This band consists of two cascades of ΔI
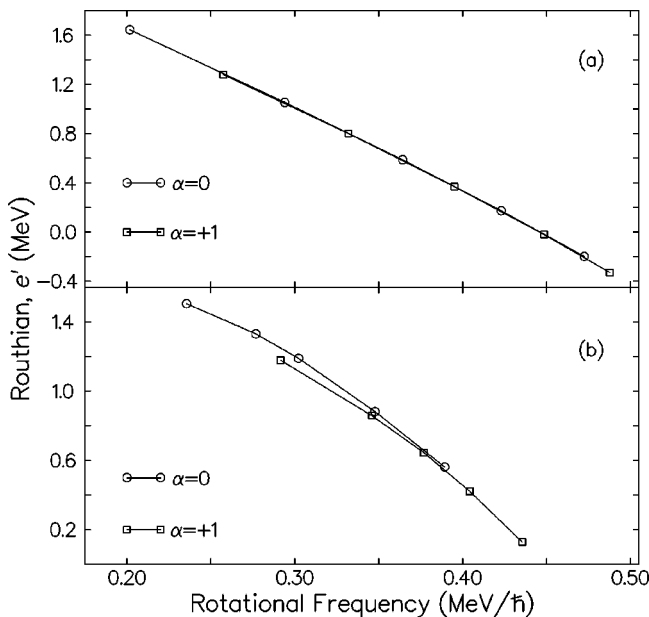
FIG. 17. Experimental Routhians e' for band 1 in ^{118}Xe (a) and band 6 in ^{116}Xe (b) calculated using the Harris parameters indicated in the caption to Fig. 9.

$=2$ transitions extending to level spins of $I^\pi=16^-$ and (19^-). Five $\Delta I=1$ mixed $M1/E2$ transitions having staggered energies connect these cascades; this staggering suggests a small amount of signature splitting. The experimental Routhians extracted for the two opposite signatures of band 6 are shown in Fig. 17(b). As seen in this figure, the signature splitting is initially about 75 keV in favor of the $\alpha=+1$ signature, and then decreases with increasing frequency. Notably, the $\alpha=0$ signature in band 6 has been observed from significantly lower excitation energies than the $\alpha=+1$ signature.

In ^{116}Xe and ^{118}Xe, there are only three negative-parity two-quasiparticle configurations which are capable of generating bands with the small signature splitting observed in Figs. 17(a) and 17(b). These are the two-quasineutron $\nu[h_{11/2}g_{7/2}]$ and $\nu[h_{11/2}d_{5/2}]$ configurations referred to earlier and the two-quasiproton $\pi[(g_{9/2})^{-1}h_{11/2}]$ configuration. So as to help identify which of these configurations are responsible for band 6 in ^{116}Xe and band 1 in ^{118}Xe, experimental ratios of reduced transition probabilities $B(M1;I\rightarrow I-1)/B(E2;I\rightarrow I-2)$ have been extracted for these bands and compared to theoretical predictions generated with the semiclassical model of Dönau and Frauendorf [47]. A description of the methods involved in this comparison has been provided in paragraph a below; a brief discussion of the interpretations which are supported by this comparison follows in Sec. IV B 2 b.

a. Analysis of experimental $B(M1;I\rightarrow I-1)/B(E2;I\rightarrow I-2)$ ratios. Experimental values for the ratios of reduced magnetic dipole and stretched electric quadrupole transition probabilities $B(M1;I\rightarrow I-1)/B(E2;I\rightarrow I-2)$ have been extracted from the measured branching ratios $I_\gamma(M1)/I_\gamma(E2)$ using the standard expression. The multipole mixing ratios δ of the $\Delta I=1$ transitions have been assumed to be small, i.e., $\delta^2 \ll 1$.

Theoretical predictions for the $B(M1)/B(E2)$ ratios have been obtained from the semiclassical model of Dönau and Frauendorf [47] using the equation

$$\frac{B(M1;I\rightarrow I-1)}{B(E2;I\rightarrow I-2)} = \frac{12}{5Q_0^2\cos^2(\gamma+30)I^2}\left[1-\frac{K^2}{(I-1/2)^2}\right]^{-2}$$
$$\times\{(I^2-K^2)^{1/2}[K_1(g_1-g_R)$$
$$\times(1\pm\Delta e'/\hbar\omega)+K_2(g_2-g_R)]$$
$$-K[(g_1-g_R)i_1+(g_2-g_R)i_2]\}^2. \quad (3)$$

In this equation, K_j, g_j, and i_j denote the K value, orbital gyromagnetic factor, and initial aligned angular momentum of the quasiparticles involved in the studied configuration, and g_R and $K=K_1+K_2$ denote the rotational gyromagnetic factor and the total K value of the configuration, respectively. The subscript 1 refers to the quasiparticle which is responsible for the signature splitting, and the subscript 2 refers to the additional quasiparticle. A value of $g_R=Z/A$ has been used for the rotational gyromagnetic factor. Orbital gyromagnetic factors g_j have been taken from the compilation of Ref. [48]. A summary of the quasiparticle parameters which have been used in calculating the theoretical $B(M1)/B(E2)$ ratios can be found in Table VIII.

TABLE VIII. Quasiparticle parameters used in calculating theoretical $B(M1)/B(E2)$ ratios in ^{116}Xe and ^{118}Xe.

Quasiparticle	g factor	K	i_x ($\hbar$)
$\nu d_{5/2}$	-0.33	2.5	0.5
$\nu g_{7/2}$	0.21	2.5	1.5
$\nu h_{11/2}$ [a]	-0.21	1.5	4.0
$\nu h_{11/2}$ [b]	-0.21	2.5	3.5
$(\pi g_{9/2})^{-1}$	1.27	4.5	0.0
$\pi h_{11/2}$	1.17	0.5	5.0

[a]In ^{116}Xe only.
[b]In ^{118}Xe only.

A simple procedure has been used to estimate the electric quadrupole moments Q_0 and γ deformations appearing in this theoretical equation. Calculations based on the TRS formalism [35–37] were performed for each studied configuration in ^{116}Xe and ^{118}Xe in order to determine the deformation parameters of the nuclear shapes. Values of the γ deformations predicted at frequencies just below the first quasiparticle alignments were placed directly into the theoretical equation, and values of the β_2 deformations predicted at the same frequencies were used to estimate the quadrupole moments Q_0 following an approximate scaling procedure. Using the quadrupole moment and quadrupole deformation of the 2^+ level in the ground-state band of ^{116}Xe as a reference, the quadrupole moment of each configuration in ^{116}Xe and ^{118}Xe was approximated by assuming a direct proportionality to the predicted deformations. While the quadrupole deformation of the 2^+ level in ^{116}Xe was predicted by TRS calculations, the quadrupole moment was determined by referring to the standard expression for the reduced transition probability $B(E2;I \rightarrow I-2)$ and the measurement of the $B(E2;2^+ \rightarrow 0^+)$ transition rate by DeGraaf *et al.* [49]. Electric quadrupole moments Q_0 and γ deformations used in calculating the theoretical $B(M1)/B(E2)$ ratios are summarized in Table IX.

Experimental $B(M1)/B(E2)$ ratios extracted for band 1 in ^{118}Xe and band 6 in ^{116}Xe are displayed together with their theoretical predictions in Figs. 18(a) and 18(b), respectively. Theoretical values have been calculated for the two-quasiparticle $\nu[h_{11/2}g_{7/2}]$, $\nu[h_{11/2}d_{5/2}]$, and $\pi[(g_{9/2})^{-1}h_{11/2}]$ configurations in ^{116}Xe and ^{118}Xe using experimental signature splittings.

b. Interpretation. As shown in Fig. 18(a), the experimental $B(M1)/B(E2)$ ratios extracted for band 1 in ^{118}Xe are

TABLE IX. Electric quadrupole moments Q_0 and γ deformations used in calculating theoretical $B(M1)/B(E2)$ ratios in ^{116}Xe and ^{118}Xe.

Nucleus	Configuration	Q_0 (e b)	γ
^{116}Xe	$\nu[h_{11/2}d_{5/2}]$	3.5	$-8.4°$
	$\nu[h_{11/2}g_{7/2}]$	3.4	$-10.6°$
	$\pi[(g_{9/2})^{-1}h_{11/2}]$	3.7	$3.3°$
^{118}Xe	$\nu[h_{11/2}d_{5/2}]$	3.6	$-12.2°$
	$\nu[h_{11/2}g_{7/2}]$	3.6	$-6.1°$
	$\pi[(g_{9/2})^{-1}h_{11/2}]$	3.8	$5.4°$
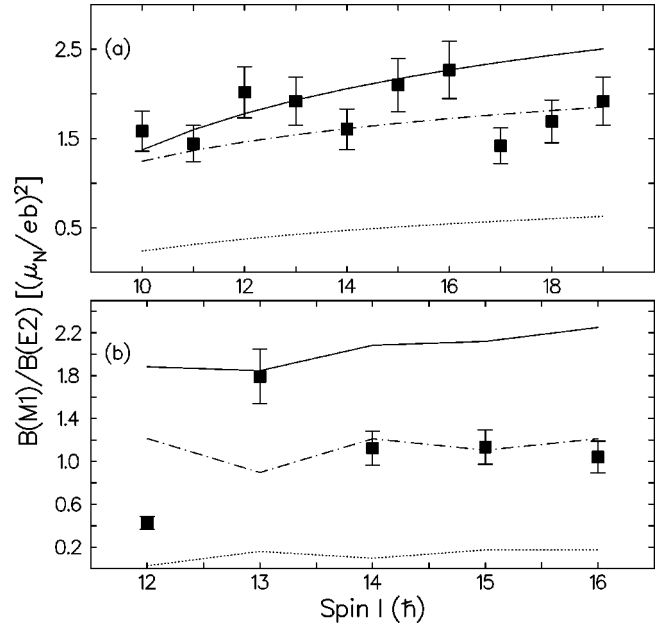
FIG. 18. Experimental ratios of reduced transition probabilities $B(M1;I \rightarrow I-1)/B(E2;I \rightarrow I-2)$ in band 1 in ^{118}Xe (a) and band 6 in ^{116}Xe (b) compared to theoretical predictions. Experimental results are denoted by solid squares, and theoretical predictions for the $\nu[h_{11/2}g_{7/2}]$, $\nu[h_{11/2}d_{5/2}]$, and $\pi[(g_{9/2})^{-1}h_{11/2}]$ configurations are indicated by a dotted, dash-dotted, and solid line, respectively.

large, having approximate values between 1.0 and 2.5 $(\mu_N/e \text{ b})^2$, and appear to be equally well reproduced by theoretical predictions for both the two-quasiproton $\pi[(g_{9/2})^{-1}h_{11/2}]$ and two-quasineutron $\nu[h_{11/2}d_{5/2}]$ configurations. An analysis of these experimental ratios using the semiclassical model of Dönau and Frauendorf was undertaken also in Ref. [23] with results similar to those presented here. In that reference, band 1 in ^{118}Xe was assigned to the $\pi[(g_{9/2})^{-1}h_{11/2}]$ configuration on the basis of the extracted $B(M1)/B(E2)$ ratios and the observed alignment behavior.

The experimental alignment i_x calculated for band 1 in ^{118}Xe is shown in Fig. 13(a) of Ref. [23]. This figure illustrates that the alignment curve of band 1 is quite smooth over the range of observed frequencies. As noted in Ref. [23], the alignment behavior of band 1 resembles that of the yrast $\pi h_{11/2}$ band in the $Z=53$ isotone ^{117}I; the alignments of both bands have large initial values, are nearly parallel with increasing frequency, and upbend near 0.40 MeV/$\hbar$. These similarities were interpreted in Ref. [23] to be indications that band 1 in ^{118}Xe has $\pi h_{11/2}$ character. As mentioned above, no new transitions have been found in band 1 in the present work. Given the alignment behaviors discussed in Ref. [23] and the comparison between theory and experiment shown here in Fig. 18(a), assignment of band 1 in ^{118}Xe to the $\pi[(g_{9/2})^{-1}h_{11/2}]$ configuration appears to be a reasonable interpretation.

Unlike band 1 in ^{118}Xe, experimental observations suggest that band 6 in ^{116}Xe does not arise from the two-quasiproton $\pi[(g_{9/2})^{-1}h_{11/2}]$ configuration. The experimental $B(M1)/B(E2)$ ratios extracted for band 6 have approximate values near 1.0 $(\mu_N/e \text{ b})^2$, which are substantially smaller than those predicted for the $\pi[(g_{9/2})^{-1}h_{11/2}]$ configuration. (Significant deviations in the experimental

values at spins $12\hbar$ and $13\hbar$ may be related to the decay pattern of the band. As shown in Fig. 1, these two spin states have additional interband decay paths which are competitive with the intraband $\Delta I = 1$ and $\Delta I = 2$ transitions.) Moreover, strongly coupled ($\Delta I = 1$) rotational bands built on configurations with a single $g_{9/2}$ proton hole tend to be characterized by very small amounts of signature splitting. As noted above, there is substantial signature splitting in band 6. Taken together, these two observations suggest that band 6 cannot be attributed to the $\pi[(g_{9/2})^{-1}h_{11/2}]$ configuration.

A two-quasineutron configuration involving the negative-parity $\nu h_{11/2}$ orbital appears to be responsible for band 6 in ^{116}Xe. As shown in Fig. 18(b), calculations for the $\nu[h_{11/2}d_{5/2}]$ configuration reproduce the magnitude of the experimental $B(M1)/B(E2)$ ratios in the band rather well, unlike calculations for the the $\nu[h_{11/2}g_{7/2}]$ configuration; this suggests the identification of the band with the $\nu[h_{11/2}d_{5/2}]$ configuration. In contrast, the signature splitting observed in band 6 favors the $\nu[h_{11/2}g_{7/2}]$ configuration. As illustrated in Fig. 17(b), the $\alpha = +1$ signature of the band is favored over the $\alpha = 0$ signature at low frequencies, even though the $\alpha = 0$ signature has been observed to originate at significantly lower excitation energies. Since the odd positive-parity neutron in the negative-parity two-quasineutron configuration responsible for band 6 involves either of the nearly degenerate $g_{7/2}$ or $d_{5/2}$ orbitals, which have opposite favored signatures, admixtures are likely. Admixtures which are known to occur between these orbitals at low spin and the competition between the orbitals' opposite favored signatures might be responsible for distorting the behavior of the observed signature splitting. Comparison between the experimental and theoretical $B(M1)/B(E2)$ ratios implies that the primary character of the positive-parity orbital in the configuration for band 6 is $d_{5/2}$. With this understanding, the band is assigned to the $\nu[h_{11/2}(g_{7/2},d_{5/2})^1]$ configuration, which involves an admixed $g_{7/2},d_{5/2}$ orbital having primary $d_{5/2}$ character.

Octupole correlations may be involved at low spin in band 6 in ^{116}Xe. The reduced transition probability $B(E1)$ of the 868-keV transition linking the $I^\pi = 8^-$ state in band 6 to the 8^+ state in the yrast band has been calculated using techniques described previously. As reported in Table VII, the $B(E1)$ rate for this transition is comparable to the rates cal-

culated for $E1$ transitions in the decay paths of bands 3 and 4 in ^{118}Xe and band 8 in ^{116}Xe; these rates were suggested above to be indicative of octupole correlations. Since the $\nu h_{11/2}$ and $\nu d_{5/2}$ orbitals having $\Delta j = \Delta l = 3$ are involved in the configuration proposed for band 6, the appearance of octupole correlations can be expected in the band. These correlations may contribute to the pattern of the observed signature splitting.

V. CONCLUSION

We have performed a thorough investigation of the nuclear structure of the even ^{116}Xe and ^{118}Xe isotopes. As a result of this work, the level schemes for these nuclei have been extended to high spins and excitation energies. In ^{116}Xe, a well-developed rotational band which manifests a gradually decreasing dynamic moment of inertia $\mathcal{J}^{(2)}$ with increasing rotational frequency has been understood within the framework of smooth band termination. Theoretical calculations suggest that this band is based upon the $\pi[h_{11/2}(g_{7/2},d_{5/2})^3]\otimes\nu[(h_{11/2})^3(g_{7/2},d_{5/2})^9]$ configuration, consistent with experimental observations. A strongly coupled ($\Delta I = 1$) rotational band attributed to the two-quasineutron $\nu[h_{11/2}(g_{7/2},d_{5/2})^1]$ configuration and a decoupled ($\Delta I = 2$) rotational band identified with the two-quasiproton $\pi[h_{11/2}g_{7/2}]$ configuration also have been found. In ^{118}Xe, previously observed bands have been extended, and several new rotational bands have been identified. The yrast band also has been revised substantially at spins greater than $26\hbar$, thereby resolving an earlier disagreement with theoretical calculations of the energy cost of high angular momenta. This work extends the knowledge about low-lying collectivity near the $Z = 50$ shell gap, and advances a systematic exploration of collectivity among the even Xe isotopes.

---

[1] R. Wadsworth, H. R. Andrews, C. W. Beausang, R. M. Clark, J. DeGraaf, D. B. Fossan, A. Galindo-Uribarri, I. M. Hibbert, K. Hauschild, J. R. Hughes, V. P. Janzen, D. R. LaFosse, S. M. Mullins, E. S. Paul, L. Persson, S. Pilotte, D. C. Radford, H. Schnare, P. Vaska, D. Ward, J. N. Wilson, and I. Ragnarsson, Phys. Rev. C **50**, 483 (1994).

[2] R. Wadsworth, H. R. Andrews, R. M. Clark, D. B. Fossan, A. Galindo-Uribarri, J. R. Hughes, V. P. Janzen, D. R. LaFosse, S. M. Mullins, E. S. Paul, D. C. Radford, H. Schnare, P. Vaska, D. Ward, J. N. Wilson, and R. Wyss, Nucl. Phys. **A559**, 461 (1993).

[3] V. P. Janzen, D. R. LaFosse, H. Schnare, D. B. Fossan, A. Galindo-Uribarri, J. R. Hughes, S. M. Mullins, E. S. Paul, L. Persson, S. Pilotte, D. C. Radford, I. Ragnarsson, P. Vaska, J. C. Waddington, D. Ward, J. N. Wilson, and R. Wyss, Phys. Rev. Lett. **72**, 1160 (1994).

[4] H. Schnare, D. R. LaFosse, D. B. Fossan, J. R. Hughes, P. Vaska, K. Hauschild, I. M. Hibbert, R. Wadsworth, V. P. Janzen, D. C. Radford, S. M. Mullins, C. W. Beausang, E. S. Paul, J. DeGraaf, A. V. Afanasjev, and I. Ragnarsson, Phys. Rev. C **54**, 1598 (1996).

[5] D. R. LaFosse, D. B. Fossan, J. R. Hughes, Y. Liang, H. Schnare, P. Vaska, M. P. Waring, J.-y. Zhang, R. M. Clark, R. Wadsworth, S. A. Forbes, E. S. Paul, V. P. Janzen, A. Galindo-Uribarri, D. C. Radford, D. Ward, S. M. Mullins, D. Prévost, and G. Zwartz, Phys. Rev. C **50**, 1819 (1994).

[6] E. S. Paul, C. W. Beausang, S. A. Forbes, S. J. Gale, A. N. James, P. M. Jones, M. J. Joyce, H. R. Andrews, V. P. Janzen, D. C. Radford, D. Ward, R. M. Clark, K. Hauschild, I. M. Hibbert, R. Wadsworth, R. A. Cunningham, J. Simpson, T. Davinson, R. D. Page, P. J. Sellin, P. J. Woods, D. B. Fossan, D. R. LaFosse, H. Schnare, M. P. Waring, A. Gizon, J. Gizon,

T. E. Drake, J. DeGraaf, and S. Pilotte, Phys. Rev. C **50**, 698 (1994).

[7] I. Thorslund, D. B. Fossan, D. R. LaFosse, H. Schnare, K. Hauschild, I. M. Hilbert, S. M. Mullins, E. S. Paul, I. Ragnarsson, J. M. Sears, P. Vaska, and R. Wadsworth, Phys. Rev. C **52**, R2839 (1995).

[8] J. M. Sears, D. B. Fossan, I. Thorslund, P. Vaska, E. S. Paul, K. Hauschild, I. M. Hibbert, R. Wadsworth, S. M. Mullins, A. V. Afanasjev, and I. Ragnarsson, Phys. Rev. C **55**, 2290 (1997).

[9] E. S. Paul, C. W. Beausang, S. A. Forbes, S. J. Gale, A. N. James, R. M. Clark, K. Hauschild, I. M. Hibbert, R. Wadsworth, R. A. Cunningham, J. Simpson, T. Davinson, R. D. Page, P. J. Sellin, P. J. Woods, D. B. Fossan, D. R. LaFosse, H. Schnare, M. P. Waring, A. Gizon, and J. Gizon, Phys. Rev. C **48**, R490 (1993).

[10] M. P. Waring, E. S. Paul, C. W. Beausang, R. M. Clark, R. A. Cunningham, T. Davinson, S. A. Forbes, D. B. Fossan, S. J. Gale, A. Gizon, J. Gizon, K. Hauschild, I. M. Hibbert, A. N. James, P. M. Jones, M. J. Joyce, D. R. LaFosse, R. D. Page, I. Ragnarsson, H. Schnare, P. J. Sellin, J. Simpson, P. Vaska, R. Wadsworth, and P. J. Woods, Phys. Rev. C **51**, 2427 (1995).

[11] E. S. Paul, H. R. Andrews, V. P. Janzen, D. C. Radford, D. Ward, T. E. Drake, J. DeGraaf, S. Pilotte, and I. Ragnarsson, Phys. Rev. C **50**, 741 (1994).

[12] I. Ragnarsson, V. P. Janzen, D. B. Fossan, N. C. Schmeing, and R. Wadsworth, Phys. Rev. Lett. **74**, 3935 (1995).

[13] A. V. Afanasjev and I. Ragnarsson, Nucl. Phys. **A591**, 387 (1995).

[14] E. S. Paul, D. B. Fossan, K. Hauschild, I. M. Hibbert, H. Schnare, J. M. Sears, I. Thorslund, R. Wadsworth, A. N. Wilson, and J. N. Wilson, Phys. Rev. C **51**, R2857 (1995).

[15] J. Bron, W. H. A. Hesselink, A. van Poelgeest, J. J. A. Zalmstra, M. J. Uitzinger, H. Verheul, K. Heyde, M. Waroquier, H. Vincx, and P. van Isacker, Nucl. Phys. **A318**, 335 (1979).

[16] H. Harada, T. Murakami, K. Yoshida, J. Kasagi, T. Inamura, and T. Kubo, Phys. Lett. B **207**, 17 (1988).

[17] M. Schimmer, S. Albers, A. Dewald, A. Gelberg, R. Wirowski, and P. von Brentano, Nucl. Phys. **A539**, 527 (1992).

[18] D. R. LaFosse, Ph.D. thesis, SUNY Stony Brook, 1994; R. S. Chakrawarthy and R. G. Pillay, Phys. Rev. C **54**, 2319 (1996).

[19] V. P. Janzen, H. R. Andrews, B. Haas, D. C. Radford, D. Ward, A. Omar, D. Prévost, M. Sawicki, P. Unrau, J. C. Waddington, T. E. Drake, A. Galindo-Uribarri, and R. Wyss, Phys. Rev. Lett. **70**, 1065 (1993).

[20] D. R. LaFosse, D. B. Fossan, J. R. Hughes, Y. Liang, P. Vaska, M. P. Waring, and J.-Y. Zhang, Phys. Rev. Lett. **69**, 1332 (1992).

[21] E. S. Paul *et al.* (unpublished).

[22] J. F. Smith *et al.* (unpublished).

[23] S. Törmänen, S. Juutinen, R. Julin, B. Cederwall, A. Johnson, R. Wyss, P. Ahonen, B. Fant, M. Matsuzaki, J. Nyberg, M. Piiparinen, S. Mitarai, J. Mukai, and A. Virtanen, Nucl. Phys. **A572**, 417 (1994).

[24] I. Ragnarsson and A. V. Afanasjev, in ''Proceedings of the Conference on Nuclear Structure at the Limits,'' Argonne, 1996, Argonne National Laboratory Report No. ANL/PHY-97/1, 1997, p. 184.

[25] J. Blachot and G. Marguier, Nucl. Data Sheets **73**, 81 (1994).

[26] K. Kitano, Nucl. Data Sheets **75**, 99 (1995).

[27] J. M. Sears, D. B. Fossan, G. Gluckman, I. Thorslund, I. M. Hibbert, R. Wadsworth, and E. S. Paul, Bull. Am. Phys. Soc. **41**(2), L11 8 (1996).

[28] J. M. Sears, D. B. Fossan, G. R. Gluckman, J. F. Smith, I. Thorslund, I. M. Hibbert, R. Wadsworth, and E. S. Paul, Bull. Am. Phys. Soc. **42**(2), B8 8 (1997).

[29] D. C. Radford, Nucl. Instrum. Methods Phys. Res. A **361**, 297 (1995).

[30] K. S. Krane, R. M. Steffen, and R. Wheeler, Nucl. Data Tables **11**, 351 (1973).

[31] B. Cederwall, A. Johnson, R. Wyss, F. Lidén, B. Fant, S. Juutinen, P. Ahonen, S. Mitarai, J. Mukai, and J. Nyberg, Z. Phys. A **338**, 461 (1991).

[32] R. Wyss, A. Johnson, F. Lidén, J. Nyberg, A. H. Nelson, D. W. Banes, A. Kirwan, D. J. G. Love, and J. Simpson, in ''Proceedings of the XXV International Winter Meeting on Nuclear Physics,'' Bormio, 1987 (unpublished), p. 542.

[33] J. F. Smith (unpublished).

[34] J. F. Smith, C. J. Chiara, D. B. Fossan, G. J. Lane, J. M. Sears, I. Thorslund, H. Amro, C. N. Davids, R. V. F. Janssens, D. Seweryniak, I. M. Hibbert, R. Wadsworth, I.-Y. Lee, and A. O. Macchiavelli, Phys. Rev. C **57**, R1037 (1998).

[35] W. Nazarewicz, G. A. Leander, and J. Dudek, Nucl. Phys. **A467**, 437 (1987).

[36] R. Wyss, J. Nyberg, A. Johnson, R. Bengtsson, and W. Nazarewicz, Phys. Lett. B **215**, 211 (1988).

[37] W. Nazarewicz, R. Wyss, and A. Johnson, Nucl. Phys. **A503**, 285 (1989).

[38] A. V. Afanasjev and I. Ragnarsson (private communication).

[39] G. Marguier, A. Charvet, J. Genevey, C. Richard-Serre, A. Knipper, and G. Walter, Nucl. Phys. **A342**, 301 (1980).

[40] J. Genevey-Rivier, A. Charvet, G. Marguier, C. Richard-Serre, J. D'Auria, A. Huck, G. Klotz, A. Knipper, and G. Walter, Nucl. Phys. **A283**, 45 (1977).

[41] R. Wyss, A. Granderath, R. Bengtsson, P. von Bretano, A. Dewald, A. Gelberg, A. Gizon, J. Gizon, S. Harissopulos, A. Johnson, W. Lieberz, W. Nazarewicz, J. Nyberg, and K. Schiffer, Nucl. Phys. **A505**, 337 (1989).

[42] T. Bengtsson and I. Ragnarsson, Nucl. Phys. **A436**, 14 (1985).

[43] J. P. Martin, V. Barci, H. El-Samman, A. Gizon, J. Gizon, W. Klamra, B. M. Nyakó, F. A. Beck, Th. Byrski, and J. C. Merdinger, Nucl. Phys. **A489**, 169 (1988).

[44] H. Timmers, J. Simpson, M. A. Riley, T. Bengtsson, M. A. Bentley, F. Hanna, S. M. Mullins, J. F. Sharpey-Schafer, and R. Wyss, J. Phys. G **20**, 287 (1994).

[45] E. S. Paul, H. R. Andrews, V. P. Janzen, D. C. Radford, D. Ward, T. E. Drake, J. DeGraaf, and S. Pilotte, Phys. Rev. C **50**, R534 (1994).

[46] S. L. Rugari, R. H. France III, B. J. Lund, Z. Zhao, M. Gai, P. A. Butler, V. A. Holliday, A. N. James, G. D. Jones, R. J. Poynter, R. J. Tanner, K. L. King, and J. Simpson, Phys. Rev. C **48**, 2078 (1993).

[47] F. Dönau and S. Frauendorf, in *Proceedings of the Conference on High Angular Momentum Properties of Nuclei*, Oak Ridge, 1982, edited by N. R. Johnson (Harwood, New York, 1983), p. 143.

[48] T. Lönnroth, S. Vajda, O. C. Kistner, and M. H. Rafailovich, Z. Phys. A **317**, 215 (1984).

[49] J. H. DeGraaf, M. Cromaz, T. E. Drake, V. P. Janzen, D. C. Radford, and D. Ward, in ''Abstracts of the Conference on Nuclear Structure at the Limits,'' Argonne, 1996, Argonne National Laboratory Report No. ANL/PHY-96/1, 1996, p. 116.